J. Membrane Biol. 147, 45–70 (1995)

The Journal of
Membrane
Biology

Sodium Channel Functioning Based on an Octagonal Structure Model

C. Sato, G. Matsumoto
Electrotechnical Laboratory, Supermolecular Science Division, Umezono 1-1-4, Tsukuba City, Ibaraki 305, Japan

Received: 6 June 1994/Revised: 29 March 1995

Abstract. The complete amino acid sequence of a sodium channel from squid *Loligo bleekeri* has been deduced by cloning and sequence analysis of the complementary DNA. A unique feature of the squid sodium channel is the 1,522 residue sequence, approximately three-fourths of those of the rat sodium channels I, II and III. On the basis of the sequence, and in comparison with those of vertebrate sodium channels, we have proposed a tertiary structure model of the sodium channel where the transmembrane segments are octagonally aligned and the four linkers of S5–6 between segments S5 and S6 play a crucial role in the activation gate, voltage sensor and ion selective pore, which can slide, depending on membrane potentials, along inner walls consisting of alternating segments S2 and S4. The proposed octagonal structure model is contrasted with that of Noda et al. (*Nature* 320; 188–192, 1986). The octagonal structure model can explain the gating of activation and inactivation, and ion selectivity, as well as the action mechanism of both tetrodotoxin (TTX) and α-scorpion toxin (ScTX), and can be applied not only to the sodium channel, but also to the calcium channel, potassium channel and cGMP-gated channel.

Key words: Squid Na channel — Ca channel — K channel — cGMP gated channel — Tertiary structure model — Voltage-gated ionic channel.

Introduction

The sodium channel is a voltage-gated ionic membrane channel essential for the generation of action potentials (Hodgkin & Huxley, 1952; Hille, 1992). The complete amino acid sequences of the sodium channels deduced by cloning and sequence analysis of the cDNAs have all been concentrated in vertebrates; that is, those from the electric organ of the eel *Electrophorus electricus* (Noda et al., 1984), from three distinct sodium channels (designated rat sodium channels I, II and III) of rat brain (Noda et al., 1986; Kayano et al., 1988), from rat skeletal muscle (Trimmer et al., 1989) and heart (Rogart et al., 1989), and human heart (Gellens et al., 1992). For invertebrate neural sodium channels, a partial amino acid sequence was deduced from *Drosophila* genomic clones isolated with a vertebrate sodium channel complementary DNA probe (Salkoff et al., 1987). Quite recently, we obtained the complete amino acid sequences of invertebrate sodium channels in squid optic lobes (Sato & Matsumoto, 1992*a*), reported in squid giant fiber lobes (Rosenthal & Gilly, 1993) and in the scyphozoan jellyfish (Anderson, Holman & Greenberg, 1993). Squid has been an important invertebrate for neurophysiology (Hodgkin & Huxley, 1952; Armstrong & Bezanilla, 1977). The squid giant axon has long been used for experiments to elucidate molecular mechanisms both of action potential generation and transmission (Hodgkin & Huxley, 1952; Tsukita et al., 1986) and of axonal transport (Vale et al., 1985). In particular, the gating mechanisms of both activation and inactivation of the squid sodium channel have been intensively studied (Armstrong & Bezanilla, 1974; Ichikawa, Urayama & Matsumoto, 1991) because squid giant axons are most amenable to voltage-clamping experiments. Experimental efforts have been focused on providing some evidence that conformational change in squid Na channel protein may accompany the gating (Landowne, 1993). The sodium channels have usually been assumed to have similar topology of structure (Noda et al., 1984; Noda et al., 1986; Kayano et al., 1988, Trimmer et al., 1989; Rogart et al., 1989; Gellens et al., 1992); four homologous domains (I, II, III and IV) containing all 6 membrane-spanning structures (S1, S2, S3, S4, S5 and S6) are repeated in tandem with 23 connecting linkers between neighboring membrane-spanning segments, and C- and N-terminals. In 1992 however, two models were presented for the struc-

Correspondence to: G. Matsumato

ture of voltage-dependent cation channels, different from the above structure originally proposed by Numa and his group; Durell and Guy (1992) proposed the model of the voltage-gated potassium channel, which introduces the links (P or H-5) between the helices S5 and S6 as transmembrane components, their antiparallel β hairpins lining only the extracellular half. We also proposed (Sato & Matsumoto, 1992*b*) a model of the sodium channel with the S5–S6 linkers as transmembrane components. In our model, the S5–6 linkers (P or H5) determine the ion-selectivity and as well, play the roles of both activation gating and voltage-sensing. The S4 segment, containing basic residues (arginine or lysine) at every third position in each domain, is widely recognized to serve as a voltage sensor (Noda et al., 1984; Kayano et al., 1988; Stühmer et al., 1989; Catterall, 1986). In our model, the S4 segments play a role quite different from that of these conventional models. Salkoff et al. (1987) also suggest from the location of the intron of the *Drosophila* putative sodium channel gene that S4 segments are located out of membrane, which is inconsistent with the previous model (Noda et al., 1986). A cytoplasmic linker between domains III and IV is mainly responsible for inactivation (Stühmer et al., 1989; Vassilev, Scheuer & Catterall, 1988; Moorman et al., 1990; West et al., 1991), in good agreement with a plug-ball model (Armstrong & Bezanilla, 1977). Furthermore, patch clamp experiments on site-directed mutants of the rat II sodium channel expressed in *Xenopus* oocytes indicate that lysine at position 1,496 (IIIS5–6) and alanine at 1,791 (IVS5–6) in S5–6 linkers are critical in determining the ion selectivity of the sodium channel (Heinemann et al., 1992), and that glutamic acid at position 403 and aspartic acid at 400 (both in IS5–6) interact directly with the pathway of the ions permeating the open channel and are closely related as the main determinants of specific binding to the blockers, tetrodotoxin and saxitoxin (Pusch et al., 1991; Terlau et al., 1991; Heinemann et al., 1992; Nakayama et al., 1992). These findings suggest that comprehensive understanding of sodium channels awaits more sophisticated progress on the sodium channel structure concept.

The present paper reports the isolation of the protein-coding sequence of the squid cDNA and the complete amino acid sequence of this novel sodium channel deduced from the cDNA sequence. The deduced sequence of 1,522 residues, approximately three-fourths of those of the rat sodium channels I, II and III, has revealed an organization virtually identical to that of the vertebrate sodium channel proteins (Sato & Matsumoto, 1992*a*). This particular simplicity of squid sodium channels facilitates the proposal of a tertiary structure model of the sodium channel. Comparisons of the amino acid sequence of the squid sodium channel are made with those of other voltage-dependent cation channels and inward rectifier K channels and cGMP-gated cation channels. In our model, Na, Ca, K channels and inward rectifier K channels and the cGMP gated channels are all included in the same family, in spite of the fact that cGMP and K channels act as homotetramers (Tempel et al., 1987; Tanabe et al., 1987; Kaupp et al., 1989; Jan & Jan, 1990). Preliminary results of our studies described here have been briefly reported (Sato & Matsumoto, 1992*a,b*).

Materials and Methods

Experimental Procedure

We adopted the PCR (polymerase chain reaction) method (Saiki et al., 1985) to isolate part of squid sodium channel gene from genomic DNA of the optic lobe of squid *Loligo bleekeri.* The live squid were captured in the Sagami Gulf of Japan and transported to the Electrotechnical Laboratory (Ichikawa et al., 1991) where they were sacrificed for the present experiments. Reaction solution for the PCR contained (in mM): 10 TRIS-HCl (pH 8.3), 50 KCl, 1.5 $MgCl_2$, and 0.01% gelatin, 200 μM NTP, 200 nM DNA primers and 25 units/ml Taq DNA polymerase (Cetus) (Saiki et al., 1988). For the DNA primers, we synthesized several 20–24 mer mixed oligonucleotides based on the amino acid sequences commonly conserved among rat I, II & III and eel Na channels, as shown in Fig. 1*a.* The DNA primers were synthesized with the Cyclone plus DNA synthesizer (Milligen). The PCR was performed in the 100 μl reaction solution containing 1 μg squid-genomic DNA with the DNA primers under the conditions of 94°C for 1 min, 54°C for 2 min and 72°C for 3 min in succession, and subjected to 50 cycles of the amplification with the thermo-cycler (Nippon Genetics). DNAs thus amplified were analyzed with 1.5% agarose gel electrophoresis. Major bands excised from the gel were ligated into the M13 mp19 vector, respectively, to be amplified and sequenced with an automatic sequencer (ABI 370A).

We also adopted the inverse PCR method (Triglia, Peterson & Kemp, 1988). For this, 1 μg squid genomic DNA was digested with 1 unit of restriction endonuclease Alu I at 37°C for 30 min, to be ligated with T4 DNA ligase. Circular DNA was used for this template to carry out the inverse PCR with the primer shown in Fig. 1*b* under the same conditions for the PCR as described above. Amplified DNA was ligated into Puc 119 and M13 mp19 vectors.

Total RNA was extracted from the squid optic lobe by the guanidium thiocyanate method (Chirgwin et al., 1979). Poly $(A)^+$ RNA was isolated by repeating oligo (dT)-cellulose chromatography twice (Pharmacia). cDNA was synthesized from 5 μg mRNA of adult squid optic lobe with reverse transcriptase (Amersham, RPN.1256Y). The cDNAs were ligated into λZAP II and transfected into XL-1 Blue cells. The cells were then inoculated into 35 culture dishes (Greiner 94/16) and transferred to the nylon membrane (Amersham, Hybond-N). The filters were treated with alkaline, neutralized and irradiated with UV to crosslink the DNA to the filter. Hybridization with the DNA probe was performed in a hybridization buffer (6× SSC, 5× Denhaldt's solution, 0.5% SDS, 20 μg/ml Salmon sperm DNA) at 65°C overnight. After hybridization, filters were washed in 0.2× SSC, 0.1% SDS at 65°C for 20 min. The insert of each clone was digested with exonuclease III and deletion mutants were sequenced. Both strands of the cDNA have been sequenced by the dideoxy chain termination method with ^{32}P labeled dCTP (Amersham) and BAS2000 (Fuji Photo Film), and further with dye-labeled oligo primer (ABI 370A).

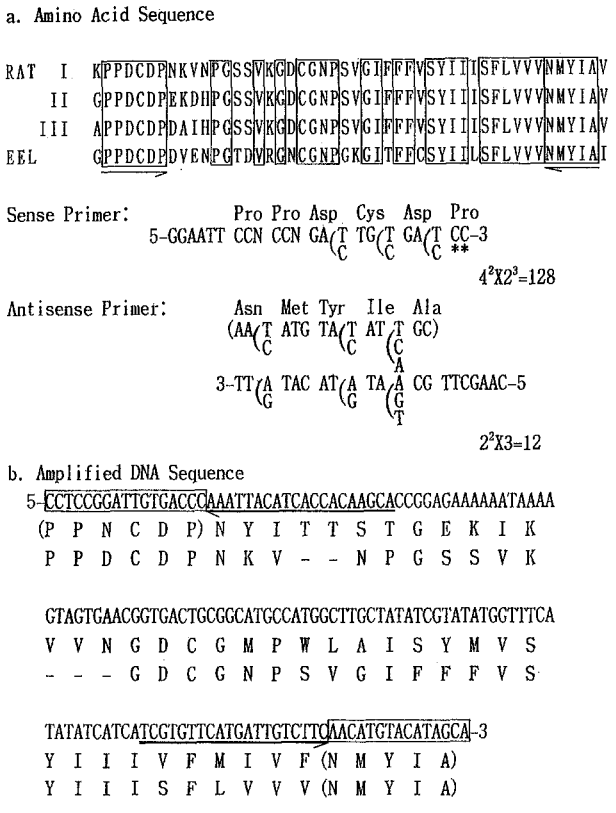

Fig. 1. The experimental procedure of PCR used for squid cDNA cloning. (*a*) The sense and antisense primers for the PCR extracted from the amino acid sequences of rat I, II & III and ell sodium channels. The sense primer of the amino acid sequence PPDCDP was used, corresponding to the one 1806–1810 between IVS5 and IVS6 (Fig. 5). The inclusion of the next two nucleotides from the amino acid[1811] is indicated by (**). The antisense primer of the amino acid NMYIA was used, corresponding to the sequence 1852–1856 in IVS6 (Fig. 5). For both primers, the degenerated combinations of codons were all synthesized for the PCR. (*b*) The sequence of DNA cloned after the PCR of squid. The nucleotide and amino acid sequences are represented at *upper* and *middle* columns, respectively, with the comparison to the amino acid sequence of rat sodium channel I (*lower*). The positions of PCR primers and of inverse PCR primers were shown with the boxes and with the arrows, respectively.

Results

Genomic PCR of the Squid

The conserved sequence of sodium channel genes was amplified with the PCR only for the IVS5–6 primers in the domain IV (Fig. 1*a*). The synthesized DNA (IVS6A) of about 150 bp (Fig. 1*b*), encoding upstream region of IVS6 and a part of IVS6 segment of the squid sodium channel, was obtained. Amplified DNA was sequenced, after it was ligated into Puc 119 vector. Following the inverse PCR was applied to the genomic DNA of squid with the primers as shown in Fig. 1*b*. DNAs were isolated and sequenced, thereby the probe IVI6 of 960 bp was acquired. With this probe, the random primed squid cDNA library in λZAP II was screened. Out of 250,000 clones, we found six positive clones, one of which was SQSR22 of 3.3 kbp. The 800 bp of SQSR22, which was located at the 5′ end, was used as the probe IV7 to obtain the cDNA clone covering the upstream region. This resulted in finding two more clones. One of them was SQSR2-7 of 3.8 kbp (Fig. 2). The restriction endonuclease maps used for the cDNA segments, SQSR2-7 and SQSR22, are shown in Fig. 2.

The Complementary DNA Sequence and Deduced Amino Acid Sequence of Putative Squid Sodium Channel

Figure 3 shows the nucleotide sequence of the cDNA, together with the amino acid sequence, for squid sodium channel 1, determined with the clones of SQSR2-7 and SQSR22. An intron was observed in IVS3 based on the genomic DNA analysis (Fig. 3). The translational initiation site was assigned to the methionine codon composed of nucleotide residues 583–585 because this is the first ATG triplet that appears downstream of a nonsense codon, TAT (nucleotides 547–549), and is contained in the nucleotide sequence ATTATGG of the residues 580–586, which has a favored sequence of A (or G) XXATGG (X representing any nucleotide) around the initiation codon ATG in the eukaryote. Thus, the open reading frame consists of 4,566 nucleotides, indicating that squid sodium channel 1 (SQSC1) is composed of 1,522 amino acids (Fig. 3) and has the molecular weight of 174,105 daltons estimated from the amino acid sequence. The 1,522 amino acid sequence is far shorter than those of vertebrate sodium channels; 2,009, 2,005, 1,951 and 1,820 for rat I, II, III and eel (Noda et al., 1984, 1986; Kayano et al., 1988). This is one of the features of the squid sodium channel. This characteristic mainly comes from the fact that the sequences exposed to the cytoplasmic side are shorter (Fig. 4). The other characteristic of the squid cDNA is AT rich since the content of AT and GC were 58 and 42%, respectively (Fig. 3).

Figure 5 shows the alignment of the amino acid sequences of squid sodium channel, as compared with those of rat sodium channels (Noda et al., 1986; Kayano et al., 1988) and the *Electrophorus* sodium channel (Noda et al., 1984). The Table shows the degrees of maximum sequence homology of squid sodium channels. For evaluation of maximum amino acid sequence homology, gaps were introduced for alignment (Table). The degree of the maximum amino acid sequence homology is 68, 67, 67, 64 and 64% for rat I/SQSC1, rat II/SQSC1, rat III/SQSC1, rat μI/SQSC1, eel/SQSC1, respectively (Table). As for another type of putative squid sodium

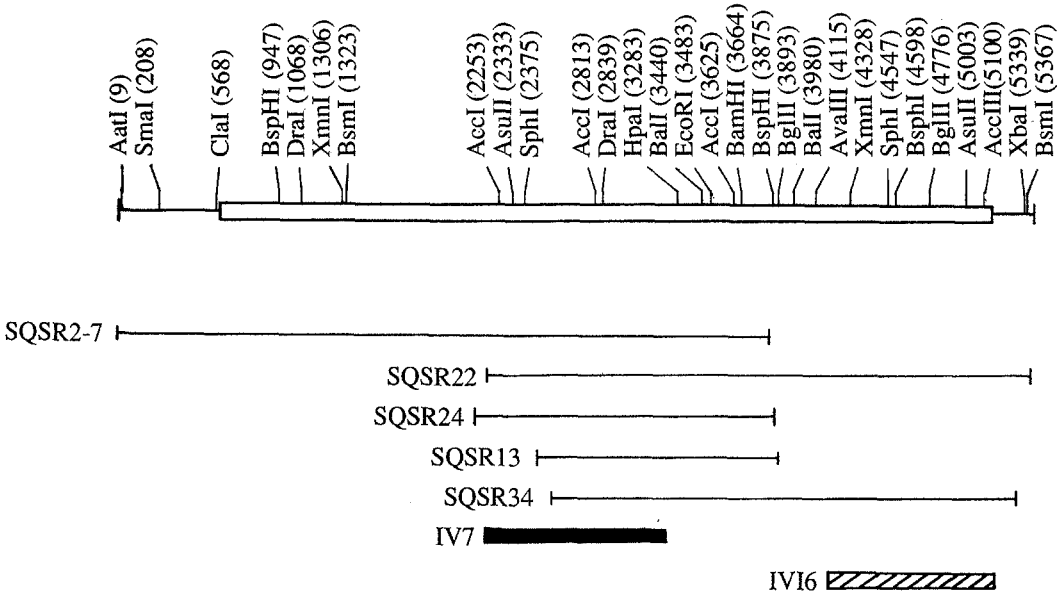

Fig. 2. Restriction endonuclease map of squid cDNAs of SQSR2–7 and SQSR22. The map stands for the cleavage sites at the 5′ terminal nucleotide by respective restriction endonucleases. Protein-coding regions are indicated by open boxes; the probe IV7 to screen upperstream is indicated by a closed box while probes IV16 is represented by hatched boxes.

channel GFLN1 (Rosenthal & Gilly, 1993), it is 62% for GFLN1/SQSC1, comparable to those of rat brain sodium channels with SQSC1 (Table). However, the degree of the nucleotide sequence homology between rat (or eel) and squid sodium channels is even lower. This could be one of the reasons why the cloning of squid sodium channel cDNA (Sato & Matsumoto, 1992*a;* Rosenthal & Gilly, 1993) has long been unsuccessful with the rat cDNAs. In fact we had tried to screen the cDNA library of squid optic lobe with the rat sodium channel cDNA which was kindly offered by Dr. M. Noda, but failed at both high and low stringencies.

It is suggested, from the comparison of the amino acid sequence of the squid sodium channel with other sodium channels (Fig. 5), that the squid sodium channel retains the same transmembrane topology as proposed for the other sodium channels (Noda et al., 1986; Kayano et al., 1988), in which the four repeated domains (I, II, III and IV) of homology, each containing the six membrane-spanning segments (S1, S2, S3, S4, S5 and S6), are successively aligned in one sequence in which the amino- and carboxy-terminal regions reside on the cytoplasmic side of the membrane. These were predicted by analysis for local hydropathicity on the deduced squid amino acid sequence (Fig. 4). Segments S1, S2, S3, S5 and S6 are apolar, while segment S4 and a linker between S5 and S6 are slightly apolar and partly even hydrophilic (Fig. 4). These are quite similar to those of vertebrate sodium channels (Noda et al., 1984; Noda et al., 1986; Kayano et al., 1988). For these characteristics of the segments, Guy and Seetharamulu (1986) proposed a model with four homologous domains but each containing eight transmembrane segments where three segments (S1, S2 and S3) are relatively apolar and two segments (S5 and S8) are quite apolar. S8 is the nomenclature that Noda et al. (1986) called S6. The close resemblance of sodium channel topology between vertebrate (human, rat and eel) and invertebrate (squid, fly and jellyfish) is consistent with the idea that sodium channel evolution took place before the separation of vertebrate and invertebrate species (Hille, 1992; Salkoff et al., 1987).

Based on the sodium channel model by Noda et al. (1986) where the sodium channel has four homologous domains, each having six transmembrane segments, S1–S6, we will compare amino acid sequence of squid sodium channel with those of vertebrate and jellyfish sodium channels in more detail (Fig. 6). For S4 segments which have widely been recognized to serve as voltage sensors (Noda et al., 1984; Catterall 1986; Guy & Seetharamulu 1986; Kayano et al., 1988; Stühmer et al., 1989), squid S4s contain 4, 3, 5 and 8 continuous basic residues which are consequently conserved (arginine R or lysine K) at every third position in the domains I, II, III and IV (Fig. 6*a*), respectively, while those of rat or eel contain 4, 5, 5 and 8 continuous basic residues at every corresponding third position (Fig. 6*a*). The difference is on IIS4 where two lysine vertebrate residues are substituted for histidine^{915} and glutamine^{918} residues in squid (Fig. 6*a*). Jellyfish S4 were revealed to contain 4, 4, 4 and 5 basic residues at every corresponding third position in tandem (Anderson et al., 1993), (Fig. 6*a*). It should be pointed out here that the basic residue at the 18th position of IVS4 of vertebrate is substituted for a negatively charged one in jellyfish, which is located in

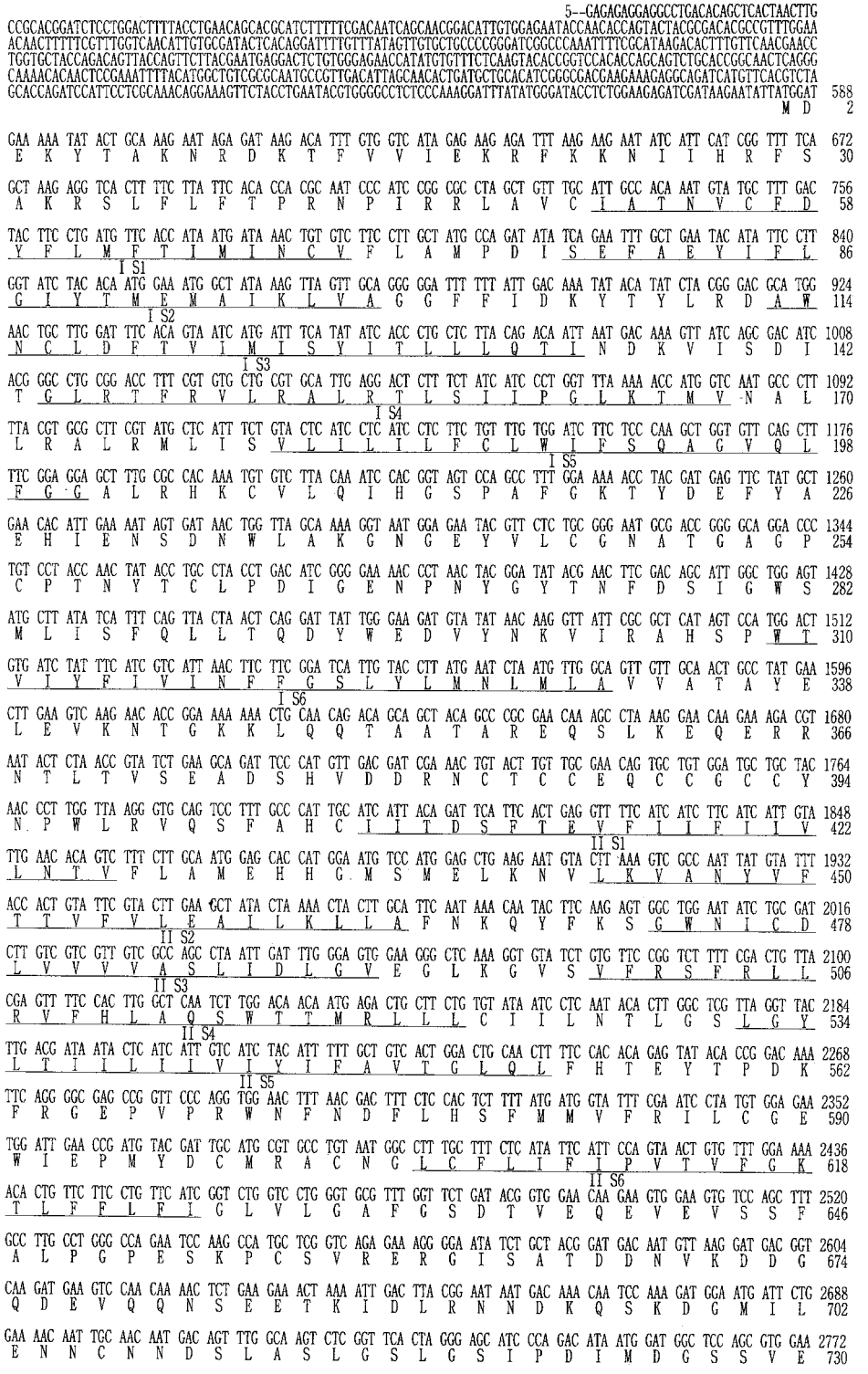

Fig. 3. Nucleotide sequence of the cDNA encoding squid sodium channel (*upper*) and its deduced amino acid sequence (*lower*). The sequence was determined with the clones of SQSR2–7 and SQSR22 (Fig. 2). Both strands of the cDNA were sequenced with either Sequenase ver 2.0 (USB) or Klenow large fragment (Takara). The nucleotide sequence is numbered, starting from the first residue of SQSR2–7. The position where an intron is inserted is indicated by arrow. This was determined by the genomic DNA analysis on the repeat IV. The Genbank accession No. is D14525.

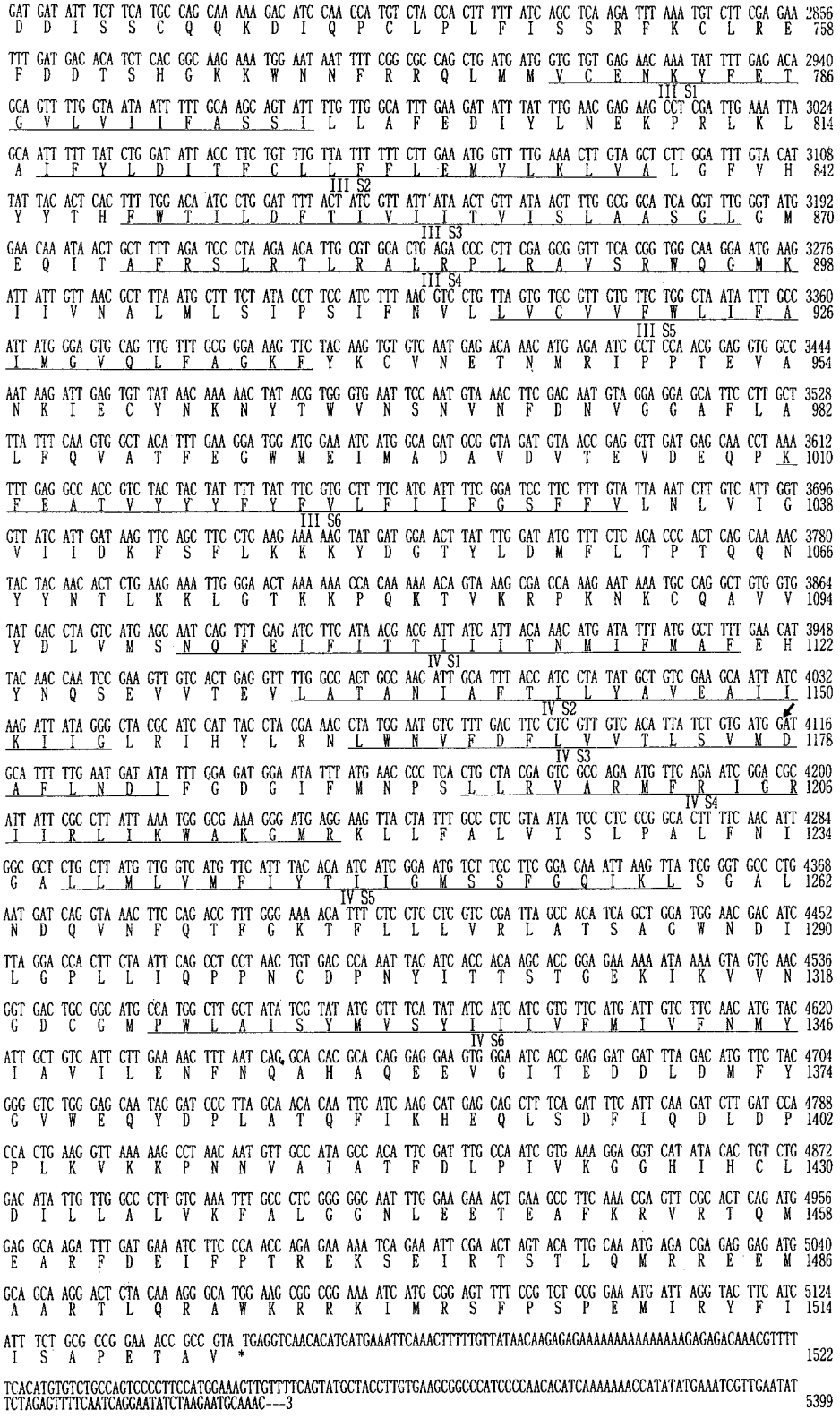

Fig. 3. Continued.

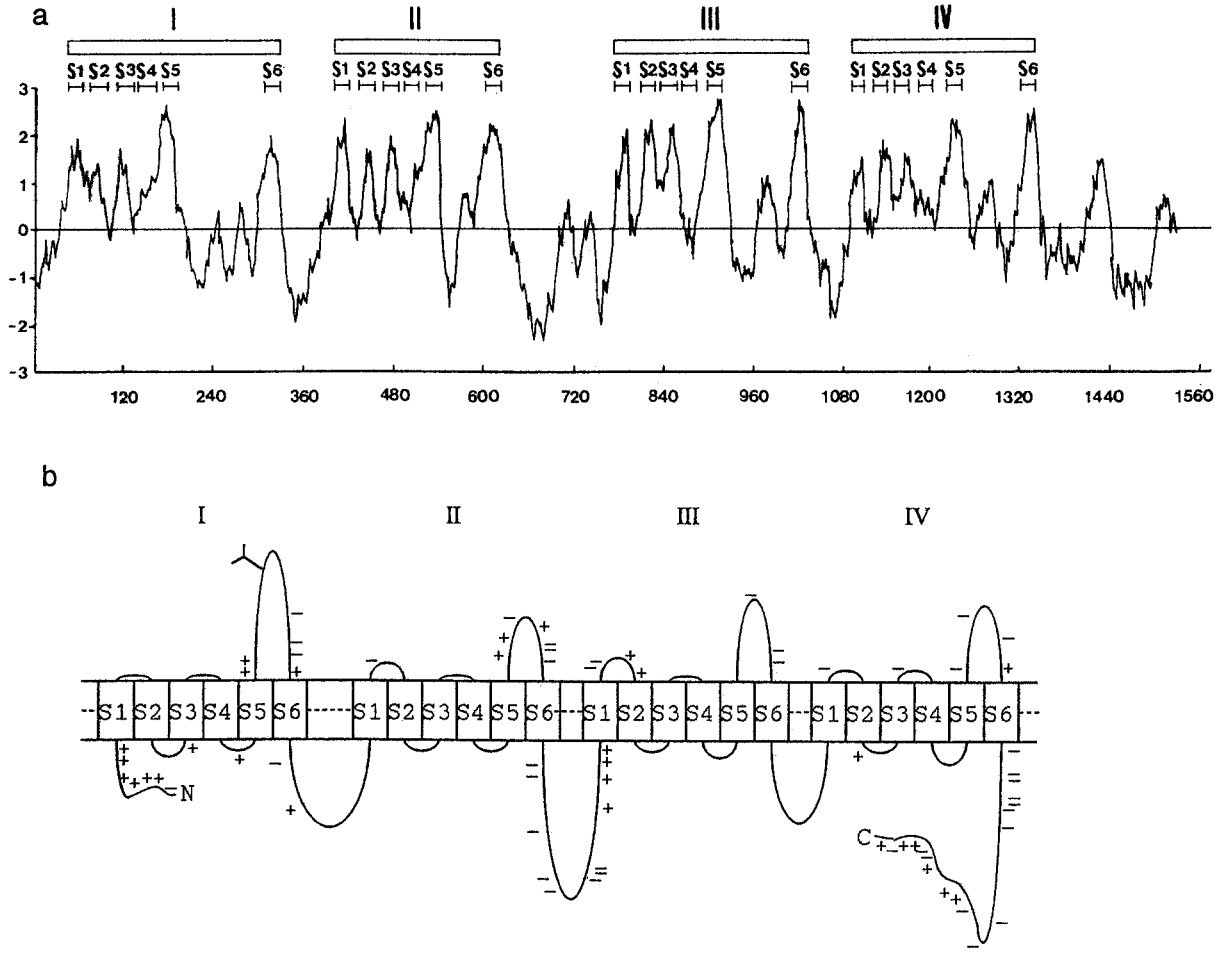

Fig. 4. Hydropathy profile of squid sodium channel and representative charge distribution of sodium channels. (*a*) The profile was obtained with use of the Kyte and Doolittle program (1982) where we ran it with a window of 19 residues. Locations of homologous repeats I, II, III and IV are indicated by open boxes. Altogether 24 hydrophobic peaks were found and indicated by their corresponding segments S1–S6. (*b*) Distribution of the positively and negatively charged residues which conserved in the outermembrane sites among squid sodium channel, rat brain I, II, III sodium channel and eel sodium channel are shown by (+) and (−) respectively in the schematics of transmembrane topology proposed by Noda et al. (1986). Potentially glycosylated site conserved between IS5 and IS6 for both squid and rat is also shown.

the middle of a positively charged spiral in the spiral models (Guy & Seetharamulu, 1986; Noda et al., 1986), and may work as an obstacle to the spiral movement. As for S2, it should be noted that glutamic acid (negatively charged) and lysine (positively charged), located in the 15th and 19th positions for each domain, are all conserved for vertebrate, squid and jellyfish sodium channels in their identical positions. In addition, segment S2 in repeats I and III contains a conserved glutamic acid or aspartic acid residue both for vertebrate and squid, which locates 10 residues upstream from the above-mentioned glutamic acid. The aspartic acid residue in jellyfish IIIS2 is, however, replaced with an asparagine residue. In jellyfish IIIS2, aspartic acid is located 3 residues upstream of the asparagine residue. Lysine^{1320} (a positively charged residue) conserved in IIIS2 for every vertebrate, which locates in the 6th position, is substituted for isoleucine^{1320} and tyrosine^{1320} in squid and jellyfish, respectively (Fig. 6*a*). Lysine in the 2nd position of IS2 in vertebrate and in jellyfish is substituted for glutamic acid in squid. Segment S3 in every repeat contains a conserved aspartic acid residue (the 6th position in each domain) for both vertebrate, squid and jellyfish at their equivalent positions. In IIS3, a negatively charged residue, 10 residues downstream from the above-mentioned aspartic acid, is conserved for both vertebrate (all glutamic acid) and invertebrate (aspartic acid). But it is noted that, in IS3, a conserved glutamic acid residue for vertebrate, located at the position 11 residue downstream from the aspartic acid (the 6th position in IS3), is substituted for leucine and methionine residues in squid and jellyfish, respectively. In IVS3, a negatively charged residue, 15 residues downstream from the aspartic acid (the 6th position in IVS3), is conserved both in vertebrate and squid but substituted for serine in jellyfish.

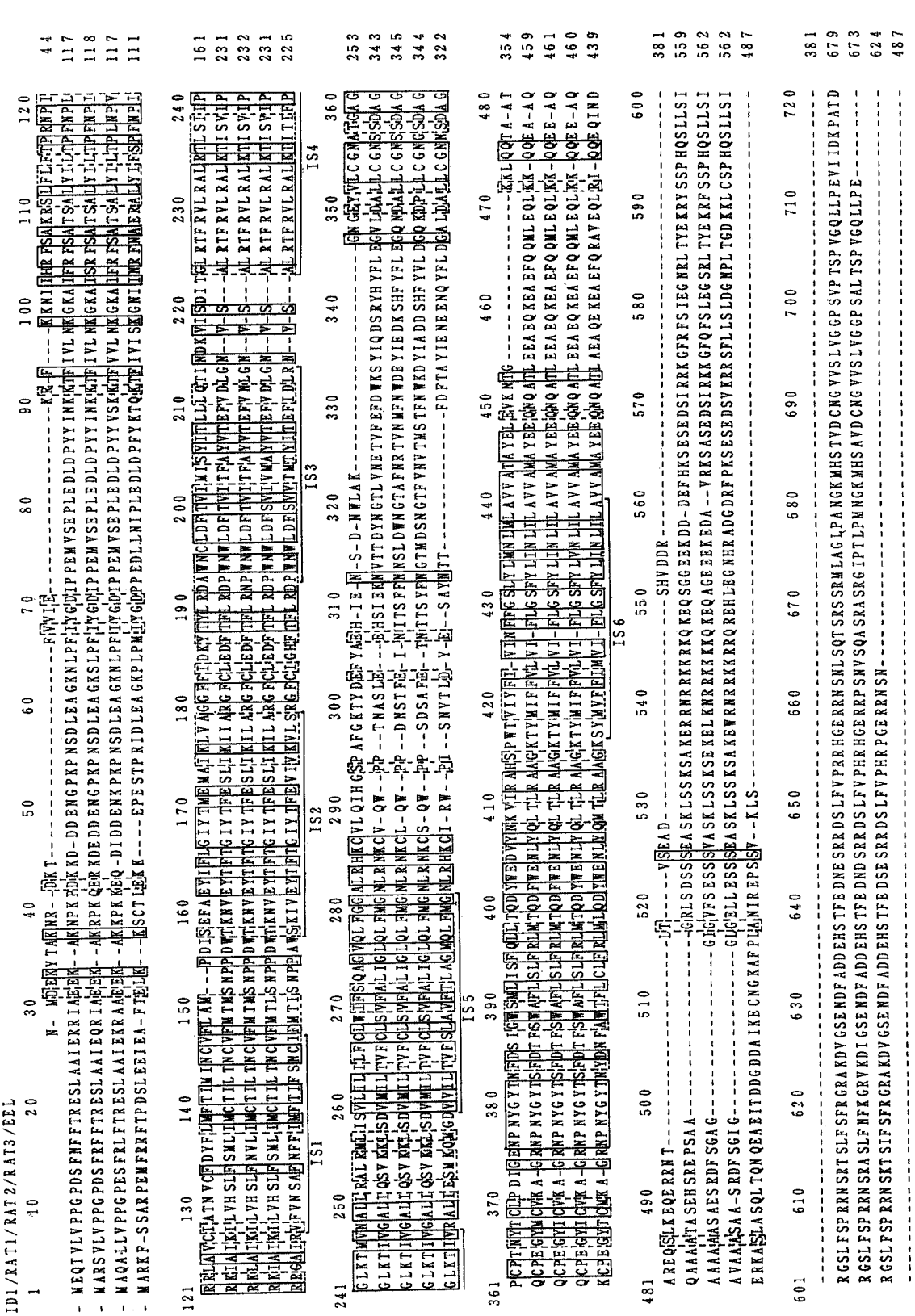

Fig. 5. Comparisons of amino acid sequence of the squid sodium channel (1st row) with those of rat I (2nd row) and II (3rd row) III (4th row) and eel *Electrophorus electricus* (5th row) sodium channels. The squid and other data are cited from Sato and Matsumoto (1992*a*), Noda et al. (1984, 1986) and Kayano et al. (1988), respectively. Identical and conservative amino acid residues are boxed with solid and broken lines, respectively. Spaces (–) are inserted into these amino acid residue alignments to achieve maximum amino acid sequence homology for all five sequences. Transmembrane segments S1–S6 are determined by the hydropathy profile analysis (Fig. 4*a*).

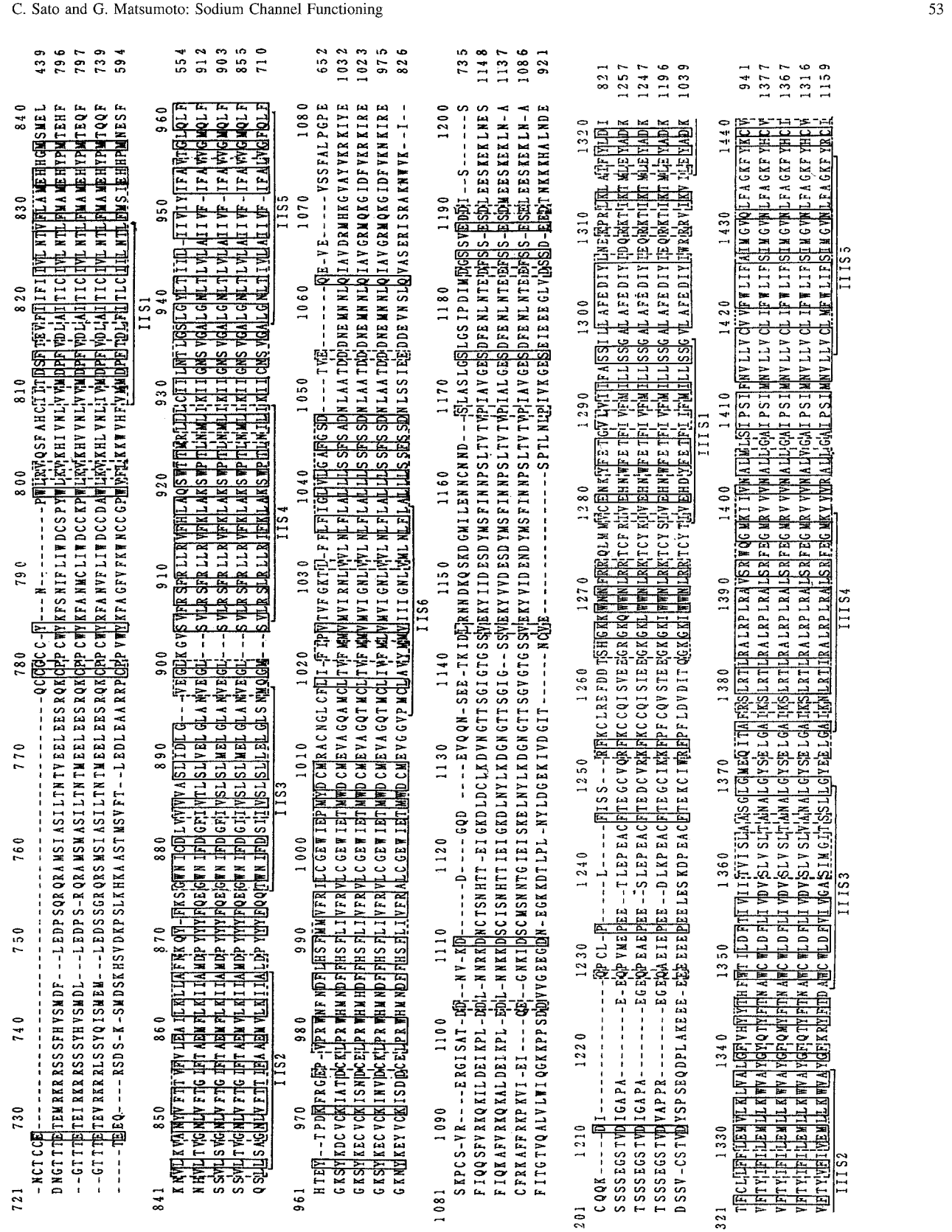

Fig. 5. Continued.

Fig. 5. Continued.

Table. Maximum amino acid sequence homology of squid sodium channels

Target/ Key	Rat brain I	Rat brain II	Rat brain III	Rat μI muscle	EEL
SQSC1	68%	67%	67%	64%	64%
GFLN1	68%	69%	67%	68%	67%

The values of target/key were acquired both from the annealed database SOUDO (Fujitsu) and from the results of DNASIS (Hitachi Software Engineering).

The cytoplasmic linker of squid between domains III and IV is quite similar in its amino acid sequence, to those of vertebrates (Noda et al., 1984, 1986; Kayano et al., 1988; Trimmer et al., 1989; Rogart et al., 1989; Gellens et al., 1992), particularly for their positively charged positions; lysine^{1554,78} residues, two successively aligned lysine^{1583,84} residues, lysine^{1587} and arginine^{1591} residues are all conserved for vertebrate, squid and jellyfish, but lysine residues^{1571,72} of vertebrate are replaced by noncharged ones, glutamine and aspargine in squid (Fig. 6*b*). A serine^{1582} residue (one residue upstream from the two successively aligned lysine residues), which can be phosphorylated in a PKC (protein kinase C) dependent manner to cause rat II sodium inactivation to slow and as well, its peak sodium current to reduce (West et al., 1991), is replaced by threonine^{1582} at the equivalent position for squid (Fig. 4, 6*b*). This suggests that the potentiality of phosphorylation at the position is conserved in squid. The phosphorylated site mentioned above is replaced by a proline^{1582} in jellyfish, indicating that it is nonphosphorylated (Fig. 6*b*). The IFM motif of III–IV linker, the quite important three successive residues for inactivation (West et al., 1992), is conserved in both squid and jellyfish as MFL and IFL, respectively. Two potentially glycosylated sites of aspargine^{312} and aspargine^{355} residues are conserved between IS5 and IS6 for both squid and vertebrate (Noda et al., 1986; Kayano et al., 1988; Trimmer & Agnew, 1989). In squid, the aspargine^{355} residue could be glycosylated but the aspargine^{312} residue could not be glycosylated because of the presence of an aspartic acid^{316} residue in its next neighbor (Hubbard & Ivatt, 1981). In squid, one more potential site of glycosylation between IS5 and IS6 is on an aspargine^{365} residue.

Octagonal Structure Model of Sodium Channel and its Functioning

In considering the tertiary structure of the squid sodium channel, we assume that all the transmembrane segments S1–S6 form not α-helices but 3_{10}-helices, because the 3_{10}-helix makes a more compact channel configuration to resist high pressure from such surrounding environments as lipids (Waugh & Hochmuth, 1987; Ito, Morton & Vodyanoy, 1989; Waugh et al., 1992) than the α-helix does. The 3_{10}-helix may be more reasonable for the channel conformation because the channel pore, a hydrophilic pathway formed inside the channel, produces a disadvantage in maintaining its structure against the pressure. In the 3_{10}-helix S4 segments, the charged side chains at every third position are clustered on one side of the helix, the opposite side being occupied mostly by nonpolar side chains (Noda et al., 1984; Sato & Matsumoto, 1992*a*). Further, when we take the charged residue configuration in S2 and S3 for all the domains of I, II, III and IV (Fig. 6*a*) into consideration, together with the peculiar positive charge configuration in S4 segments, an octagonal structure can be obtained that is most stable, as illustrated in Fig. 7Ad. The S4 segments form to make a hydrophilic pore, with their positively charged residues faced to the pore. S2 segments also form the specific pore, with negatively charged residues in the 15th position facing the pore. It should be noted that S2 segments are not highly apolar as a whole. Further, it is noted that the positively charged residue in the 19th position of S2 segments are closely coupled with the negatively charged one in the 6th of S3 segments because they are neighbors or quite close to each other, as counted in the amino acid numbers from cytoplasmic side: 4 and 6 residues away from the cytoplasmic end of the respective segments (Fig. 6*a*). The negatively charged residue in the 8th position of IIS1 is also closely coupled with a positively charged one at the 19th position of IIIS4: 8 and 6 residues from the cytoplasmic side, respectively. S1, S5 and S6 segments, all hydrophobic, surround the core formed by S2, S3, S4 segments, and stabilize the octagonal core structure. In this conformation, S1 through S6 segments of the each repeat are organized one-way around (Fig. 7*Ad*). This model matches reasonably with the length of the linker between the segments: the minimum lengths of the linkers for squid and rat brain I, II and III sodium channels are 7, 8, 3, 9, and 51 in their residue numbers for S1–2, S2–3, S3–4, S4–5, and S5–6 linker, respectively (Fig. 4).

In the synthesis process of the channel protein, the channel protein could not form the octagonal structure at its initial stage of the tertiary structure formation. Noda et al. (1986) proposed a tertiary structure model of the sodium channel in which S4 is surrounded by the other five segments in each repeat. This organization seems to be basically stable for each isolated repeat even when we adopt 3_{10}-helices for trans-membrane segments (Fig. 7*Aa*). In the 3_{10}-helix assumption, it is noted that charge positions in 3_{10}-helices (Fig. 7*B*1 or 6) are quite different from those in α-helices by Noda et al. (1986). After all the amino acids of the sodium channel are completely synthesized, the transitional structure of the channel under the synthesis would be unstable enough to induce structural changes. The six most allowable stable con-

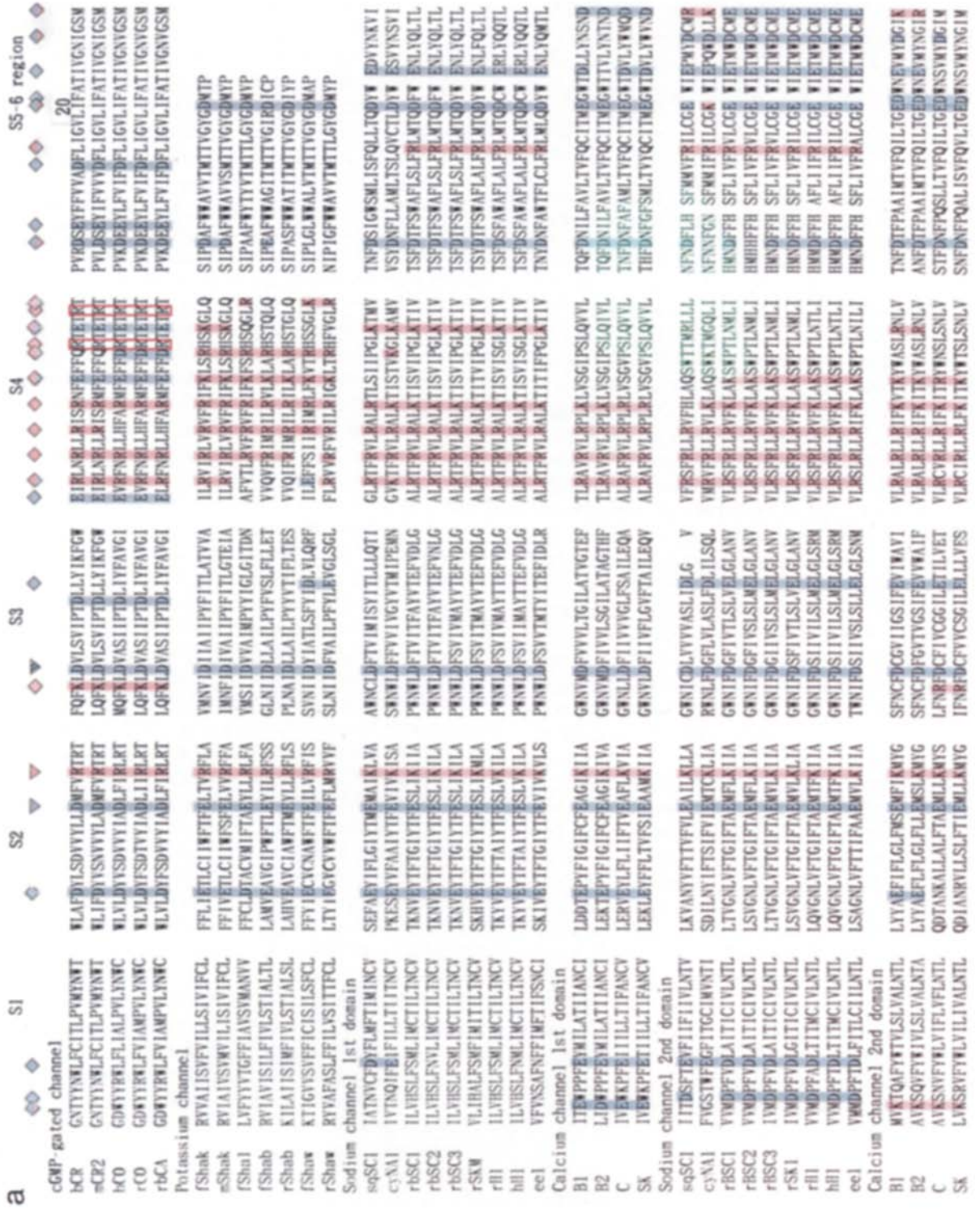

Fig. 6. Detailed comparisons of amino acid sequence for S1, S2, S3 and S4 segments and the S5–6 regions in bovine (bCR) and mouse (mCR2) retinal cGMP gated, and bovine (bCO) and rat (rCO) olfactory cAMP gated, and rabbit aorta (rbCA), cNMP gated channel, Drosophila Shak (f Shak), mouse *Shak* (m *Shak*), f *Shal,* f *Shab,* rat *Shab* (r *Shab*), f *Shaw* and rodent *Shaw* (r *Shaw*) potassium channel, and domains I, II, III and IV of squid (sqSC1), jellyfish (cyNA1), rat I (rBSC1), rat II (rBSC2), rat III (rBSC3), rat Skeletal muscle (rSKM) and heart (rH1), human heart (hH1) and *Electrophorous electricus* (eel) sodium channels and of rabbit brain (B1, B2), Skeletal (Sk) and Cardiac (C) calcium channels (*a*). Detailed comparisons for III–IV linker of sodium channel (*b*). The data are cited from Noda et al., 1984; 1986; Tanabe et al., 1987; Tempel et al., 1987; Tempel, Jan & Jan, 1988; Kayano et al., 1988; Butler et al., 1989; Frech et al., 1989; Kaupp et al., 1989; Mikami et al., 1989;Rogart et al., 1989;

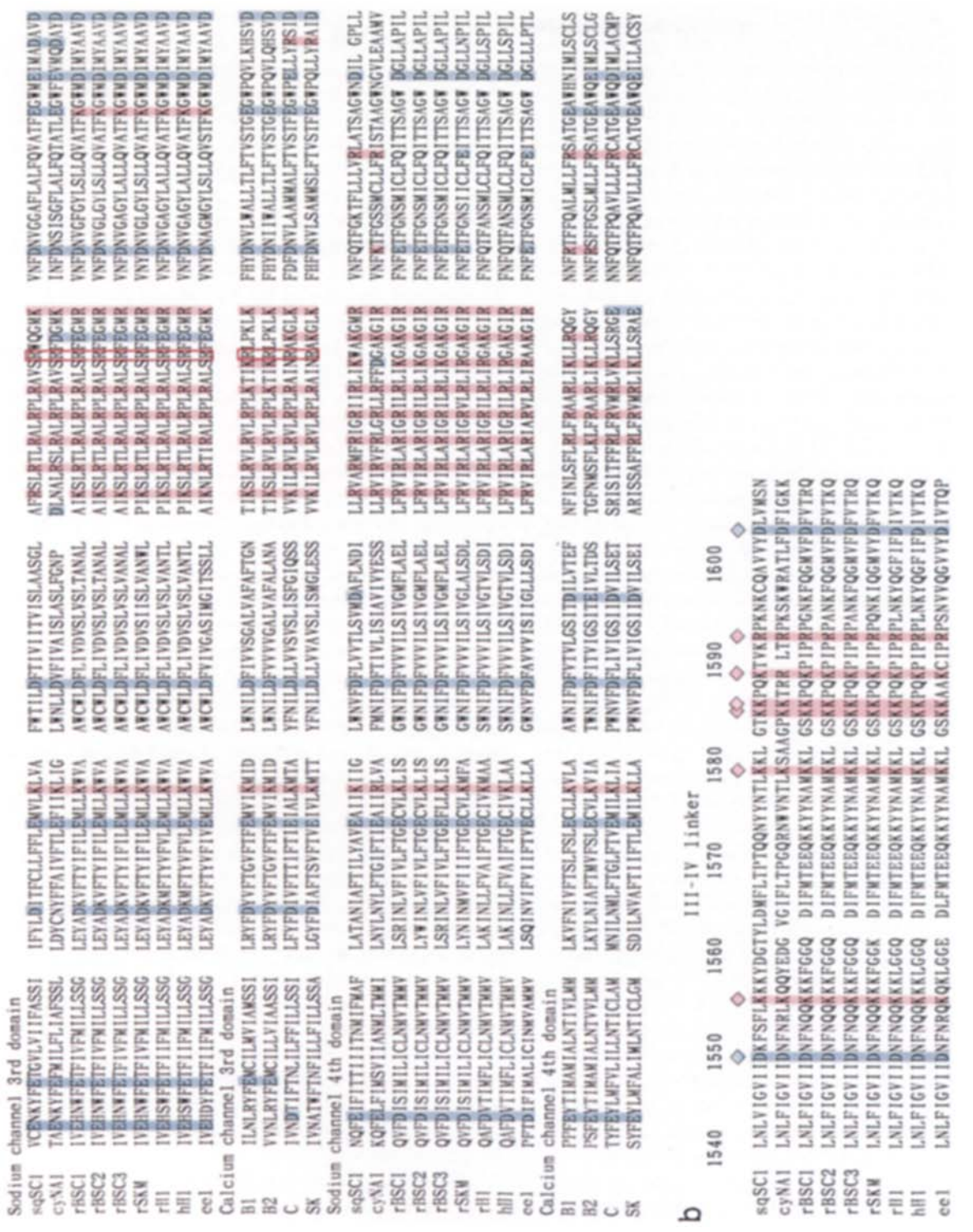

Fig. 6. Continued. Trimmer et al., 1989; Yokoyama et al., 1989; Dhallan et al., 1990; Ludwig et al., 1990; Wei et al., 1990; Mori et al., 1991; Gellens et al., 1992; Niidome et al., 1992; Pittler et al., 1992; Sato & Matsumoto, 1992*a;* Anderson et al., 1993; Biel et al., 1993. Homologous amino acid residues are aligned vertically to be in the same positions by inserting spaces. The positions of identical and conservative charges of any channels are indicated by hatched and open triangles, and that of conservative ones in a domain of a kind of channel by open square, respectively. Positively and negatively charged residues at the positions mentioned above are boxed with red and blue squares, respectively, and the marks mentioned above are also colored like the residues. Positively charged residues where the positions do not fit the rule of the position multiplied by 3 in S4 are boxed with red lines.

figurations are shown in Fig. 7. The Noda model is represented in Fig. 7*B*1 or 6. In this assembly of repeats, the four isolated blocks of repeats move rapidly to the lateral direction in the membrane, and align in a stable conformation in Fig. 7*Ab*. The charges of each repeat cylinder determine the rotational organization of the configuration, as judged from the requirement that the electrostatic energy becomes minimum. The charges essential for the rotational organization are the negatively charged residues in the 5th position of S2 segments characteristic of both I and III repeats, and Asp^{890} in the 16th position of IIS3, and positively charged one in the 19th of IIIS4, and negatively charged ones in the 8th of IIS1 and IIIS1, and negatively charged ones in the 3rd of IIIS1 and the 4th of IVS1. Six conformations are possible as a result of the stability consideration where S2 locates nearest to the center and S3 in the next nearest position (Fig. 7*B*). This is because these S2 and S3 segments are not highly apolar (Fig. 4). S2 segments are most important to determine the rotational orientation in the assembly because it possesses one positively charged residue and one or two negatively charged ones. Another negative charge of IIS3 is additionally important to determine the rotational orientation by the electrostatic interaction with S2 segments. The configuration, thus assembled, of Fig. 7B5 or 7*Ab*, which is I-IV-II-III in a clockwise-rotated configuration as viewed from extracellular side, is the most stable among the six configurations of Fig. 7*B*. This most stable configuration resulted from the situation that neighboring domains (IV and II; II and III; III and I) are electrically coupled to lower the electrostatic energy. Furthermore, it is noted that total positive charges of S4 in III and IV are larger than those of S4 in I and II (Fig. 6*a*), with the result that the electrically repulsive force between III and IV is larger than that between I and II. Therefore, the conformation where III and IV repeats neighbors is not energetically favorable. In the configuration of Fig. 7*Ab* where III and IV are oppositely faced, I and IV repeats are loosely coupled through the weak electrical interaction. On the other hand, for the intradomain coupling of IV domain, S4 is tightly bound to S1, S2 and S3. This is because the positive charges on S4 strongly couple with the negative charges on S1, S2 and S3, respectively (Fig. 7*Ab*). In addition, a positively charged site on IVS4 is attracted to a negative charge on IS2 which is not directly coupled with the positive charge of IVS4 at the initial transitional states up to *b* in Fig. 7. In other words, the structural change is assisted by the coupling between the IVS4 positive charge and IS2 negative charge. With the electrostatic interaction and together with the hydrophilic atmosphere, IVS4 moves towards the center of the channel. In this situation, repeat I is pushed out from the configuration *b* for IVS4 to be repositioned between IS2 and IVS2 (Fig. 7*Ac*). Then, IS2 moves toward IVS4 through the attractive interaction between the negative charge on IS2 at the cytoplasmic side and the positive charges on IVS4 (Fig. 7*Ac* and *d*). The movement of IS2 accompanied by this reconfiguration produces the spatial gap between IS2 and IS3. At the same time, negative charges in IIIS1, IIIS2, IS2 and IS3 attract IS4. As a result, IS4 is reconfigured between IS2 and IIIS2 (Fig. 7*Ac* and *d*). Then, IIIS4 and IIS4 are integrated to form a specific pore with hydrophilic atmosphere of its inner surface (the core) in succession. The overall rearrangement of the channel configurations takes place as a structure transition through the configurations a → b → c → d in Fig. 7*A*, to stabilize an octagonal structure of the Na channel (Fig. 7*Ad*). In the octagonal structure, the S5–6 regions, composed of 30, 29, 31 and 40 residues located between S5 and S6 in domains I, II, III and IV, respectively, are stabilized by interacting with the inner surface of the core formed by the S4 and S2 segments. The S5–6 regions are most probably at the extracellular side of the membrane before the octagonal channel structure is formed. Then, the S5–6 regions could be pushed into the core after the octagonal structure is formed. There is another possibility that the S5–6 regions are already integrated partly into the membrane before the octagonal structure is realized and then transferred to the inside of the core during the process of rearrangement of the channel structure formation. It is noted that the S5–6 regions serve a strongly negative-charged moiety; that is, the total effective charge number in the S5–6 regions is 9 as a nominally negative charge (in other words, the difference between negatively and positively charged residues in S5–6s as a whole) in squid, and 10–11 in rat brain type I–III (Noda et al., 1984, 1986; Kayano et al., 1988). The core of S2 and S4 possesses strong positive charges in a straight line between extra- and intracellular sides and facing its inner surface, with its pore diameter estimated to be 0.5–1.5 nm, i.e., wide enough to accept the S5–6 regions inside it (Fig. 8*f*). The S5–6 regions can be partly integrated into the pore in the resting state of the sodium channel, presumably up to the positions where the negatively charged residues of the S2 segments (designated as the stopping residues) are located, resulting in the stabilization of the octagonal structure of the channel (Fig. 8*b, c, d, f*). More concretely, the tips of the S5–6 regions in the resting state remained at the positively charged sites of their respective S4 located nearest to the stopping residues.

In our model of the sodium channel, the S5–6 region plays a principal role in activation gating, voltage sensing and ion-permeable selectivity. (i) The respective S5–6 region makes a loop from the outside to the inside and back again, forming the ion-selective channel. The four S5–6 regions are all negatively charged as a whole, and it can be hypothesized that they are antiparallel hairpin forms, with their tips negatively charged (Fig. 8). All these negative charges can sense membrane potentials so that S5–6 regions play the role of voltage sensing.

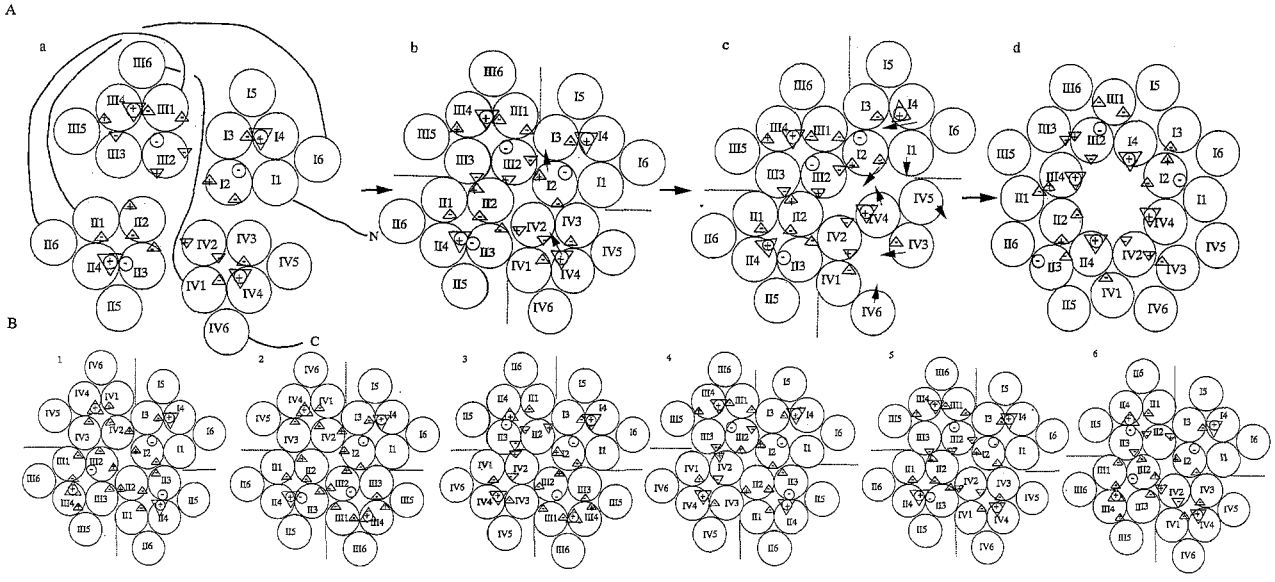

Fig. 7. Schematic illustrations of the self-organization process of the channel, as viewed from the extracellular side. (*A*) Rearrangement of segments is schematically represented to form the stable conformation, the functional "Octagonal core structure of the channel." Border of each domain is shown with broken line. (*a*) channel structure with the domains of I–IV–II–III arrangement in clockwise order is more stable than the one of I–II–III–IV which was adopted from Noda et al. (1986). (*b*) The arrangement of I–IV–II–III repeats causes minimum repulsive energy among other arrangements with the same domain configuration as shown in 6 cases of B. This arrangement is identical to the case B5. (*c*) Transitional state of the domain configuration change. The domain arrangement I–IV–II–III is unaltered, and (*d*) the stablest conformation of the channel structure "Octagonal core structure". (*B*) Six states of rotationally-organized configurations in which the conformation of six transmembrane segments in each domain is identical to the one adopted from Noda et al. (1986). The charges surrounded with circles and triangles stand for those positioned in the extracellular and cytoplasmic sides of the channel, respectively.

This is quite in contrast with the view that S4s are voltage sensors (Noda et al., 1984, 1986; Catterall, 1986; Kayano et al., 1988). Instead, in our present model, S4s, together with S2s, form a guiding pore through which the S5–6 regions can slide. The S4 segments may act as a rail for the S5–6 train. Positive charges in S4 segments of I, II, III repeats are partly lacking near the cytoplasmic side. The spatial gap length, dependent on the number of missing positive charges on the rail, is quite influential in determining the voltage dependency of the channel activation, together with the negative charges of the S5–6 region. This gap also contributes to prohibit the channel from opening spontaneously in the resting membrane potential. This model agrees well with the site-directed mutagenesis experiment by Stühmer et al. (1989) where neutralization of the positive charge in the middle of S4 regions generally causes slow activation, but neutralization of the nearest charge to the extracellular side does not influence the voltage dependency of the sodium channel activation. (ii) This model agrees well with the result that the S5–6 can determine the ion selectivity (Heinemann et al., 1992). The negatively charged residues of the S5–6 linkers could select permeable ions through the pore formed by the four S5–6 regions, together with its pore size (Hille, 1992). In Fig. 6*a*, the alignment data show the gaps characteristic to each repeat in the S5–6 regions of sodium channels; 23rd position of IS5–6 and 8th and 21st of IIS5–6 in all sodium channels, but 23rd of IVS5–6 only in vertebrate. This determines the spatial distribution of negative charges in the channel (Fig. 6*a*). In contrast, the model of Durell and Guy (1992) cannot explain why anions are not permeable in the channel in the resting (closed) state (Miller, 1993). (iii) In the resting state, the tips of antiparallel hairpin S5–6 regions partially enter into the S4–S2 pore up to a position which forms a balance with the attractive force that is due to positively charged residues of S4, and at the same time, with the repulsive force due to negatively charged residues of S2 (Fig. 8*c, d*). The repulsive force partly comes from both the resting membrane potential and the carboxyl terminal segment which possesses a strong negative charge as a whole (27 negatively and 23 positively charged residues in squid sodium channels) since in our model the C-terminal segment is located at the mouth of the S4–S2 pore on the intracellular side in the resting state (Figs. 8 and 9). This configuration is reasonable because both resting membrane potential and the positive charges on S4 cylinders plug the negatively charged C-tail into the S4–S2 pore. This conformation is further stabilized by the III–IV linker which is highly positive (13 positively and 4 negatively charged residues in the III–IV linker of the squid sodium channel), and surround the C-tail from the cytoplasmic side in the resting configuration (Fig. 8). The

position of the III–IV linker forms a balance with the repulsive force due to both the positively charged center pore and resting membrane potential and with attractive force due to the negatively charged C-tail as illustrated in Figs. 8 and 9.

Upon depolarization, the S5–6 region further slides into the S4–S2 pore to the cytoplasmic side along the "linear rail" of S4 cylinders, depending on the membrane potential (Fig. 9*a, b*). The activation energy required for the respective S5–6 region to pass through the pore is determined basically by the electrostatic interaction between a S5–6 region and its associated S4 segment wall which might behave as a complete rail of IVS4 but as some incomplete rails of other S4s (Fig. 8*c, d, f*). The activation energy also depends on the distance between the tip of the S5–6 region and the negatively charged C-tail surface facing the core pore initially (under the resting state environment). The IVS5–6 region can pass through the S4–S2 pore with the least energy since the IVS4 segment, possessing the completely periodic lining of 8 positively charged residues at every third position, gives the least activation energy for the S5–6 region to pass through the pore. The S5–6 regions for domains III and I follow the IVS5–6 since the noncharged residues between the positively charged residues of IIIS4 and IS4 at every third position are less in number than those of IIS4. Lastly, the IIS5–6 moves to the cytoplasmic side because of its highest activation energy. As the S5–6 regions approach the cytoplasmic side, the C-tail which has covered the S4–S2 pore from the cytoplasmic side, is removed by both of the electrically repulsive interactions between negative charges of the C-tail and those of the S5–6 regions, and between negatively charged C-tails and the membrane potential (Fig. 9b). The C-tail thus removed from the pore is most likely to be attracted to the N-terminal region (Fig. 9*c*) because the N-terminus is positive-charge rich (14 positively and 4 negatively charged residues in squid; *see* Fig. 5). The other possible sites to which the C-tail is attracted are the II–III linker, IS2–3 and IS4–5 regions, which are all positive-charge rich (nominally 4 positive charges among the last 26 bases for the II–III linker, one positive residue^{190} and one positive residue^{254} for S2–3 and S4–5, respectively). These are illustrated in Fig. 9. The nominal charge of N-terminal region, C-tail, III–IV linker and the last 17% of II–III linker in squid were +10, –4, +9, and +4, respectively. When the four S5–6 regions pass through the S4–S2 pore to form an ion-selective channel and the C-tail is completely removed so that cations can pass through (Fig. 9*c*), the activation is completed.

Accompanied by the activation in which the S5–6 regions pass through the S4–S2 pore to the cytoplasmic side and the C-tail is repelled from the pore, the III–IV linker, which has been well understood to play a crucial role in inactivation (Vassilev et al., 1988; Stühmer et al., 1989; Moorman et al., 1990; West et al., 1991), moves away from the channel together with the C-tails (Fig. 9*b*). It should be noted that the III–IV linker in our model covers the S4–S2 pore by crossing it diagonally (Figs. 8 and 9). In the configuration of the activated state (Fig. 9*c*), the III–IV linker interacts more strongly with positively charged sites of the C-tail than when it is in the resting state (Fig. 9*a*), because some negatively charged sites of C-tail start to connect to positively charged sites of the N-terminal region. The III–IV linker in this acti-

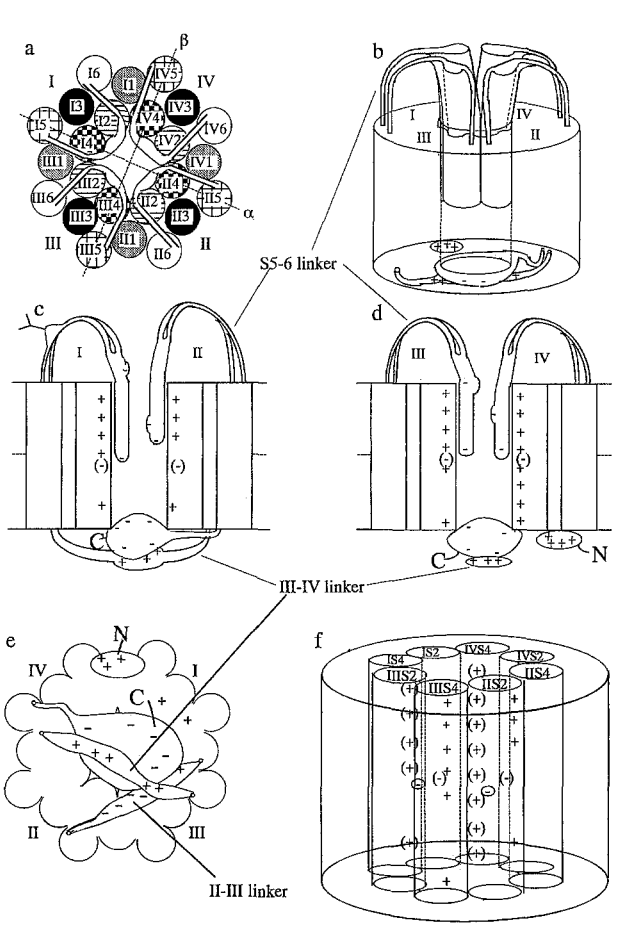

Fig. 8. Schematic illustrations of our proposed tertiary structure model of sodium channel. Octagonal topology of transmembrane segments S1–S6 and the S5–6 regions for the domains I–IV is shown, as viewed from the extracellular side (*a*) and from the transmembrane side (*b*), respectively. Resting configurations of the S5–6 regions, C- and N-terminals and III–IV link are also illustrated along line α (*c*) and line β (*d*) where cross sections of the segments (I and II) and (III and IV) are viewed, respectively. The putative glycosylation site is also shown. Resting configuration of the C- and N-terminals and II–III and III–IV link are also illustrated, as viewed from the cytoplasmic side (*e*). Distribution of charged residues in the lining of the core pore formed by S2 and S4 segments of the squid is shown as viewed from membrane side (*f*), where ones in IIS2 and IIIS2 are surrounded with circle. The charged residues in I and IV repeats are surrounded with parentheses. S5–6 region is not shown here (*f*).

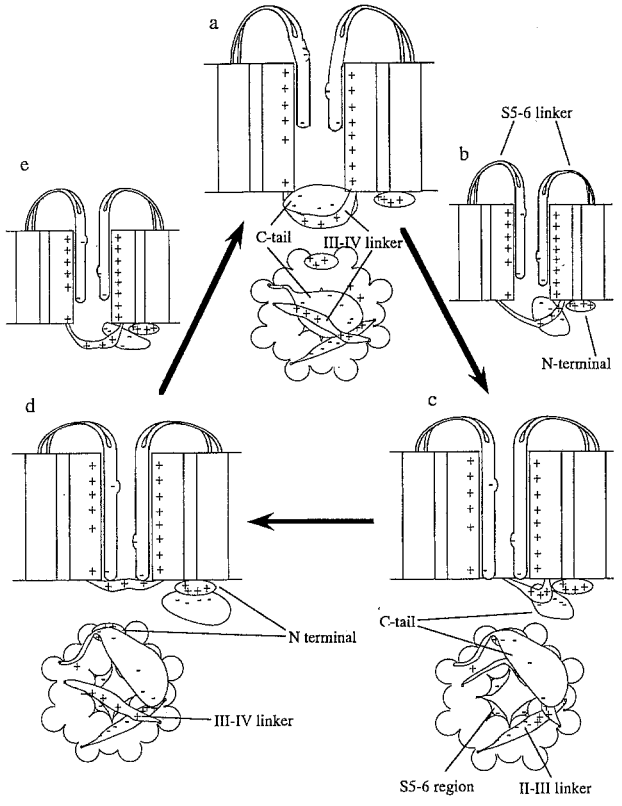

Fig. 9. Schematic illustrations of a proposed tertiary structure model of the sodium channel corresponding to the resting (*a*), initially activated (*b*), fully activated (*c*), inactivated (*d*), restoring resting (*e*) states, respectively. The *upper* and *lower* pictures for each drawing represent the transmembrane and intracellular side views of the channel, respectively.

vated configuration is both electrically and elastically unstable, since it is attracted by the negative charges at the tip of the S5–6 pore (Fig. 9*c, d*). Therefore, it eventually reaches the inactivated configuration (Fig. 9*d*). In other words, the inactivated state is the virtual stable configuration when the S5–6 linkers reach the cytoplasmic side, resulting in the III–IV linker interacting with the S5–6 regions electrostatically to cover the S5–6 pore. On repolarization to the resting membrane potential, the C-tail is attracted to the membrane side, and eventually, the III–IV linker is attracted to the original (resting) cytoplasmic side (Fig. 9*e*). As a result, the C-tail interacts with the III–IV linker again, leading to the original resting configuration (Fig. 9*a*). The C-tail in the resting configuration is favorable directly by the action of the membrane potential itself and also by the S5–6 regions away to the extracellular side.

Discussion

General Characteristics of our Octagonal Structure Model of Sodium Channels

The present paper has described our proposed tertiary structure model of the squid sodium channel and its function. In this model, the S5–6 regions play an essential role in (i) sensing membrane potentials, (ii) forming the ion-permeable pore, specifically and selectively, for sodium ions, and (iii) functioning as the main part of the activation gate. The C-tail also works in activation gating, together with the S5–6 regions in a collective fashion. The III–IV linker plays a crucial role in inactivation, as has been well established by others (Vassilev et al., 1988; Stühmer et al., 1989; Moorman et al., 1990; West et al., 1991; McClatchey et al., 1992). Our model has further described a molecular mechanism of the coupling between activation and inactivation, which has been in question since Armstrong and Bezanilla (1977) discovered the coupling from their measurements of sodium gating currents using squid giant axons. Armstrong and Bezanilla (1977) revealed that inactivation immobilizes almost ⅔ of the gating particles. The close interaction of S5–6 regions to the III–IV linker in the inactivated state in our octagonal structure model might explain the activation-inactivation coupling. Moorman et al. (1990) reported that neutralization of lysines in the III–IV linker of rat III sodium channels by their site-directed mutagenesis experiments causes rapid inactivation. In our model, this experiment is explained well by the specific interaction between the III–IV linker and the C-tail; that is, the number of positively charged residues which electrically couple with the negative charge of C-tail in our model is decreased by the substitution experiment.Then, the inactivation III–IV linker is released rapidly from the C-tail through both electric and elastic interaction. The hinged-lid model proposed by West et al. (1992) might emphasize the importance of elastic force caused by hinged structure where site directed mutagenesis to break the hinge structure may deprive the elastic force from the III–IV linker. In conclusion, our model characterizes well, by the movement of the charged residues in S5–6 regions and C-tail, the qualitative features of the gating current of sodium channel activation and inactivation (Bezanilla, 1985; Armstrong & Bezanilla, 1977).

Our proposal that the S5–6 regions form the ion-permeable and selective pore may be supported by other experiments employing site-directed mutagenesis and also by the photoaffinity-label experiment (Nakayama et al., 1992); substitution of a single residue in the S5–6 region renders rat sodium channel II insensitive to tetrodotoxin (TTX), and markedly reduces its single channel conductance (Noda et al., 1989; Pusch et al., 1991; Terlau et al., 1991). This kind of point mutation also renders cardiac sodium channels sensitive to TTX (Satin et al., 1992), and alters the ion selectivity like calcium channels when K is changed to E, and A to E in the 20th position of III and IVS5–6 region of rat brain sodium channel, respectively (Heinemann et al., 1992). Further, the single point reverse mutation in human cardiac calcium channels increases its sodium permeation (Tang et al.,

1993). Here it is noted that the amino acid corresponding to the residue K of rat IIIS5–6 region was revealed to be E, both in squid (Figs. 3 and 5; Sato & Matsumoto, 1992*a*) and jellyfish (Anderson et al., 1993). It was experimentally established that the squid sodium channel is permeable to Ca ion to some extent (Baker, Hodgkin & Ridgway, 1971). Here we note that the transcriptional products of SQSC1 gene were experimentally detected clearly in squid giant axons (Sato, Hirota & Matsumoto, 1995). In squid, A^{1791}, in the 20th position of IVS5–6 region was identical to that of the vertebrate. However, E^{1009} in the 31st position of IIS5–6 and A^{1504} in the 28th position of IIIS5–6 region in vertebrate are substituted for R and D in squid, respectively (Fig. 6*a*). These changes might almost compensate for the effect of the substitution of the residue in the 20th position of IIIS5–6 region. These indicate that the total tertiary structure of S5–6 region is related to the ion selectivity. Here it should be noted that jellyfish sodium channels are TTX insensitive (Anderson, 1987). However, the amino acid sequence of jellyfish S5–6 region was shown to possess every known character of a TTX sensitive sodium channel (Anderson et al., 1993). It supports the importance of the total S5–6 tertiary structure for the ion selectivity.

One of the most prominent peculiarities of our model is the dynamic characteristic of the S5–6 regions; that is, the S5–6 regions can move, depending on the membrane potential. This dynamic character is quite consistent with the experimental finding that the ion selectivity is markedly voltage dependent, and that it is reduced and enhanced upon hyperpolarization and depolarization, respectively (I. Seyama, *personal communication;* Hironaka & Narahashi, 1977). The S5–6 pore should become more strongly ion-selective when it enters into the cytoplasmic side on depolarization. This is qualitatively well understood as shown in Fig. 9. The dynamic characteristic of the S5–6 regions can also be supported by the experiments that TTX blocks not only sodium ionic current but also reduces the sodium activation gating current (Ichikawa et al., 1991; Keynes et al., 1991). In other words, TTX affects not only ion-permeable pathways but also sodium activation gates. This experimental finding can be explained only by our model (Fig. 10*c*). Our model, showing that the S5–6 regions work as activation gates, is also quite consistent with the finding that a peptide toxin of *Leiurus* scorpion (ScTX) binds to certain localized sites in the IS5–6 region (Tejedor & Catterall, 1988; Thomsen & Catterall, 1989) in a voltage-dependent manner or as a function of the steady state of activation (Catterall, 1979). ScTX may bind to the site which is located in an extracellular part of S5–6 region in the resting state (Fig. 10*a*), and the bound toxin may prevent the S5–6 region from protruding to the cytoplasmic side enough to crosslink to the III–IV linker (Fig. 10*c*). In our model, the III–IV linker correlates directly with the C-tail which closely interacts

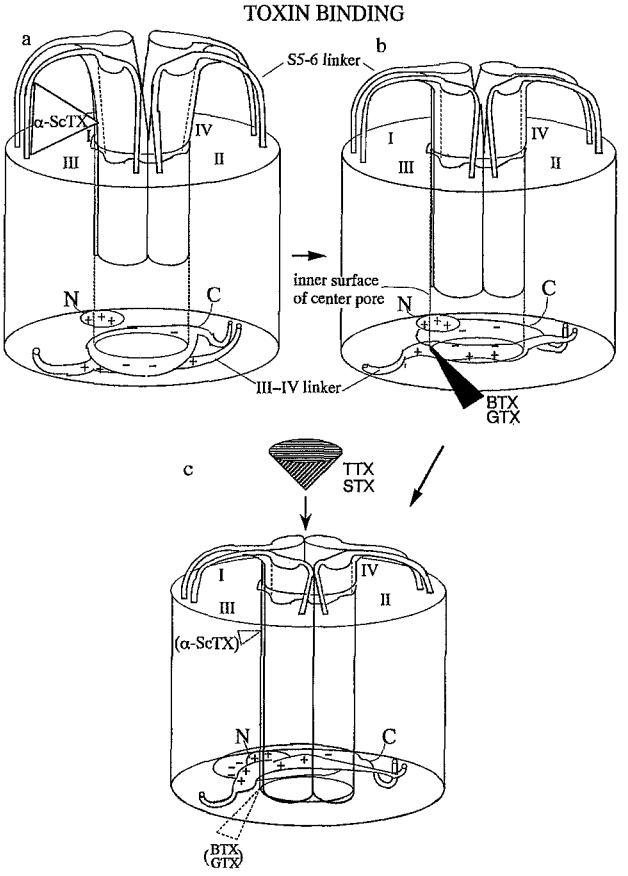

Fig. 10. Schematic illustrations of binding sites of toxins specific to sodium channels including tetrodotoxin (TTX), saxitoxin (STX), α-scorpion toxin (ScTX), batrachotoxin (BTX) and grayanotoxin (GTX). a. The ScTX binding site and its functional relation. In the resting state, ScTX, shown by the open triangle, binds to the IS5–6 region to prevent the IS5–6 region from reaching the cytoplasmic side. This blocks to induce the inactivation, as explained in the text. (*b*) Action of BTX or GTX. At the initial activated state, BTX or GTX, shown by the filled triangle, binds to the positively charged residue on the cytoplasmic side of S4 segment in the center pore. Penetration of BTX or GTX into the center pore is only possible when C-tail is just disconnected from the pore and S5–6 region does not reach to the charged residue yet. (*c*) Action of TTX or STX. In the excited state, TTX or STX, shown by the hatched cone, plug the center pore of the channel.

with the S5–6 regions. This assumption may also be supported by the Moorman et al. experiment (1990) showing that the mutation of arginine to glutamic acid in the III–IV linker of rat III sodium channel made inactivation rapid, and at the same time, delayed activation. Our model can expect this delayed activation: substitution of one positive residue in the III–IV linker to the negative one crucially influence the C-tail conformation through the interaction between the III–IV linker and the C-tail. The negative site of the C-tail, originally coupled with the positive one of the III–IV linker before the substitution, is repelled from the original position after

the substitution of the negative residue, and most probably faced the S5–6 linkers. This produces a larger electric repulsion force between the S5–6 region and C-tail, resulting in the delayed activation in the opposite side of the III–IV linker.

Stühmer et al. (1989) reported that neutralization of the positive charge[225] in the 3rd position of IS4 near the extracellular side by site-directed mutagenesis did not influence the kinetics of activation and that the neutralization of one of the positive charges[228, 231, 234] in the 6th, 9th, 12th position resulted in the delay of the activation. The experiments can be understood well by assuming that S4s play a role as the charged rail for the S5–6, rather than by assuming that S4s are voltage sensor. In our model, it can be understood that delayed activation is caused by higher activation energy for the S5–6 region to pass on the IS4 rail with the missing charge at every third position. It is also reported by Auld et al. (1990) that the site-directed mutagenesis of noncharged residues, leucine to phenylalanine, of S4 segment in rat IIA sodium channel dramatically alters its gating property. This may also be explained in our model in such a way that the physical shape of the S4 rail affects the movement of the S5–6 train.

Both Batrachotoxin (BTX) and Grayanotoxin (GTX) are known to activate the sodium channel. The molecular moiety of the sodium channel facing the D-ring of GTX is suggested to be rich in positive charges (Tsuji et al., 1991). In our model, a target site of GTX is located at the cytoplasmic end of the sodium channel core which is positively charged, especially the 24th residues of III and IVS4 (Fig. 6*a*), disconnecting the C-tail from the cytoplasmic end of the center pore (Fig. 10*b*). It is well known that the ion selectivity becomes highly reduced when the sodium channel is activated by BTX (Khodorov, 1978) or by GTX (Tsuji et al., 1991). Our model can explain the ion selectivity reduction in such a way that both BTX and GTX open the channel without inserting the S5–6 regions into the S2–S4 pore. It is also well established experimentally that there is a cooperative action between ScTX and BTX; ScTX enhance the activation of the sodium channel by BTX (Catterall & Beneski, 1981). Here it should be noted that experiments have confirmed that both BTX and GTX bind their target sites on the activated state. Therefore, for the BTX-activation of sodium channel, where the C-tail is removed from the center pore at the cytoplasmic side, this accessibility of BTX to the S4s facing the cytoplasmic side happens by chance through thermal fluctuations of both C-tail and S5–6 regions. ScTX works to enhance the probability by binding to the S5–6 regions, resulting that BTX is more accessible. (*See* Fig. 10*b*).

Noda et al. (1984, 1986) also discussed the possibility of both α- and 3_{10}-helices as the structural candidates for the possibility of both α- and 3_{10}-helices as the structural candidates for the transmembrane segments of the sodium channel. They finally adopted the α-helix structure. On the other hand, we selected the 3_{10}-helix which might be more advantageous in channel proteins.

Durrel and Guy (1992) proposed in their model that most of the membrane spanning S4 protrudes to the outside of the membrane by the helical movement when the channel is in the activated state. This does not seem energetically advantageous because S4s possess mostly hydrophobic residues other than the conserved positive charges. The least energy necessary to activate the sodium channel is calculated to be about 3 kcal/mol in BTX-modified sodium channel (Chabala et al., 1991). On the other hand, the activation energy is rather small to induce a structural change in the channel. Furthermore, in the activated state of their model in which the S4s are protruded to the extracellular side of the membrane, the center pore could not be protected against the pressure of the membrane. Our model qualitatively solves these difficulties. Furthermore, their model could not explain why the reduction of the membrane potential from –60 mV to –40 mV is enough for the activation of the channel. Our octagonal structure model requires only a small reduction of the membrane potential, not necessarily a reversal potential to activate the sodium channel.

Squid Sodium Channels

Rosenthal and Gilly (1993) reported another subtype of squid sodium channel protein. They deduced the amino acid sequence from GFLN1 sequence. The sequence was derived partly from nucleotide sequence of a cDNA clone PNZ5. But, the remaining sequence was determined from PCR fragments only. In the GFLN1 sequence, they intentionally deleted four nucleotides, AAGT, a part of the nucleotide sequence between the I and II repeat from PNZ5 clone. This nucleotide sequence resulted from other short PCR products. According to their explanation, this is because stop codons are involved in original PNZ5 nucleotide sequence after I repeat. Generally, nucleotide sequences determined by PCR products are considered to be unreliable compared with those of cDNA. Because they deleted a part of their sequence from short PCR products, the sequence should be experimentally confirmed with the long cDNA clone. Further, it should be stressed here that the insert AAGT, inducing frame shift in PNZ5, does not match the general intron splicing rule, GT-AG rule; that is, the first two bases of the introns should be GT and the last two bases be AG (Lewin, 1994). The possibility of a pseudogene can not be excluded for GFLN1.

They also compared their amino acid sequence with those of vertebrates and reported that GFLN1 shows a higher similarity to vertebrate sodium channels than SQSC1 does. However, the degree of the maximum homology between vertebrate sodium channels/SQSC1 and

between vertebrate sodium channels/GFLN1 is analyzed in detail here and summarized in the Table, that shows that they are almost similar. SQSC1 resembles rat brain sodium channel types I and II maximally and to muscle channel types minimally. It is quite consistent with the experimental fact that SQSC1 mRNA is specifically expressed in squid neural tissues (Sato et al., 1995). As for IIS4, they pointed out that the histidine and glutamine found in the 12th and 15th positions of IIS4 in SQSC1, respectively, corresponding to the two lysine residues in vertebrate IIS4, might cause poor voltage sensitivity. However, histidine is known also to be classified as a basic amino acid and positively charged according to its micro-environment (Conn et al., 1987). Furthermore, it should be noted that, to complement the weakly positive residue and glutamine, SQSC1 possesses one positively charged residue in the 21st position of IIS4 (Fig. 6a). Jellyfish sodium channel CYNA1 also lacks the positively charged residue in the 15th position but possesses the positive one in the 18th position. This compensation effect is quite reasonable for our model, since positive charges in S4 closer to cytoplasmic side are more effective for the activation gating than the positive charges located near to the extracellular side.

Relationship of our Model to Other Cation Channels in the Same Family: cGMP Gated Channel, Potassium Channel and Calcium Channel and Inward Rectifier Potassium Channel

Our model can be extended to the calcium and potassium channels, and, as well, the cGMP gated channel in the following ways: (i) These channels conserve S1–6 segments and S5–6 regions quite similarly to those of the sodium channel (Fig. 6*a*). Charges most responsible for the octagonal structure formation are the positive charge in the 19th position of S2 and the negative one in the 6th position of S3. All these charges are commonly conserved at the identical positions of the sodium channels so far cloned. At the same time, stopping residues of S2 and negatively charged S5–6 regions were all conserved as well, and positively charged residues of S4 are well conserved as a whole. (ii) Either C-tail or N-tail has a strong negative-charge in total. (iii) In calcium channels, negatively charged residues in the 5th position of IS2 and IIIS2 and in the 16th of IIS3 and in the 4th of IVS1, that determine the rotational orientation of four repeats in the octagonal model, are conserved at their identical positions, respectively. In contrast, voltage-gated potassium channel and cGMP-gated channel, consisting of homotetramers (Tempel et al., 1987; Kaupp et al., 1989), do not conserve the negatively charged residue in the corresponding position to the 4th of IVS1, and in the 16th of IIS3 except Shaw potassium channels (Fig. 6*a*). (iv) The S5–6 regions of the potassium and calcium channels are also thought to be located near or in the center pore, depending on the membrane potential. These data were obtained by site-directed mutagenesis experiments in which substitution of a single amino acid in the S5–6 region altered toxin sensitivity and/or ion selectivity (MacKinnon & Yellen, 1990; Yellen et al., 1991; Kim et al., 1993; Tang et al., 1993). (v) Furthermore, ion-selectivity of one potassium channel was voltage-dependent like that of the sodium channel (French & Wells, 1977; Bezanilla & Armstrong, 1972). This may suggest the S5–6 of potassium channels function in a similar way to that of the sodium channel in our model.

S5–6 regions conserve negatively charged residues in the 4th position in all the channels in this family except ones in f *Shal* and r *Shab* and *Shaw* K channels and in repeat IV of calcium channels and in II and IV repeats of some kinds of sodium channels (Fig. 6*a*). However, the negatively charged residues in the 20th, 24th and 31st positions in S5–6 regions were partly conserved, with a pattern that is characteristic of each kind of channel (Fig. 6*a*). cGMP-gated channel conserves the negatively charged residues in the 4th, 6th, 13th positions, while the potassium channel does in the 20th and partly in the 4th. The calcium channel conserves negatively charged residues in the 20th position in every repeat, in the 4th one in only repeats I, II and III, in the 31st one in I and III, and in the 21st one in II. As a result, the numbers of the charged residues in S5–6 region per domain of cGMP-gated channel, potassium channel, calcium channel and sodium channel are nominally −2.8 (−3 ~ −2), −1.29 (−2 ~ −1), −2.33 (−2.75 ~ −1.5) and −2.56 (−3.25 ~ −2.25) in average, respectively, whereas the numbers of S4 are 1.8 (1 ~ 3), 5.86 (4 ~ 7), 5.92 (5.25 ~ 6) and 5.75 (5.5 ~ 6) in average, respectively (Fig. 6*a*). The differences between the absolute values of these two values are −1.25 (1 ~ −2), 4.57 (3 ~ 6), 3.58 (3.25 ~ 3.75), 3.19 (2.25 ~ 3.75). As for S4, the total charge value of the K channel is almost the same as those of Na and Ca channels, however its gating kinetics is not so fast, compared with those of the Na channel. As for the S5–6 region, it is noted that the charge value of the potassium channel is lowest among those channels. These may favor the idea that the voltage sensor is in the S5–6 regions rather than S4, and that S5–6 regions play an essential role in activation.

It should be stressed that cGMP-gated channels have only little voltage sensitivity (Kaupp et al., 1989), but it conserves the S4 segment. cGMP-gated channels possess four positively charged residues at the conserved position near the extracellular side of S4, but not near the cytoplasmic side. In the S4 segments two residues in 15th and 21st positions, and sometimes one residue in the

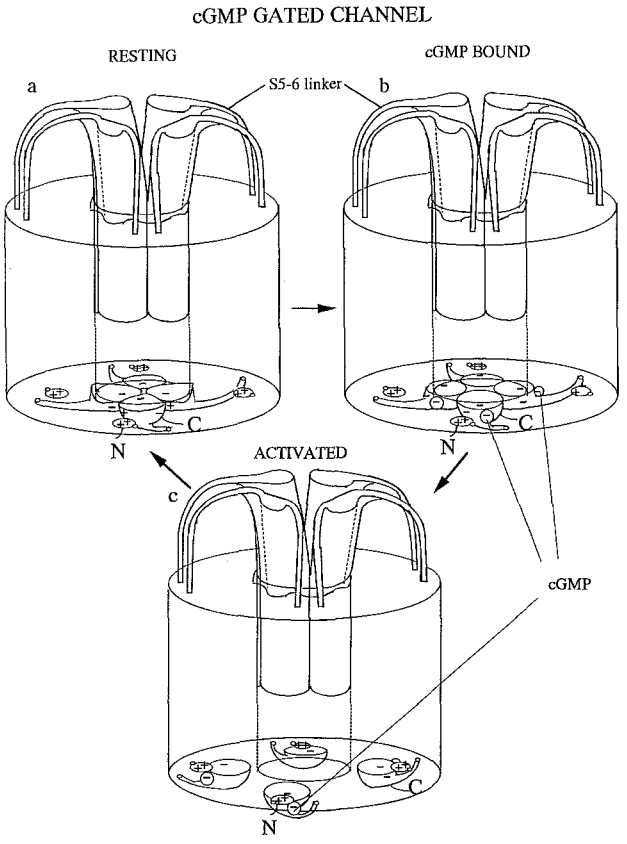

Fig. 11. Schematic illustrations of the cGMP gated channel structure of the resting (*a*), initially activated (*b*) and fully activated (*c*) states. cGMP is shown as a circle including a minus mark. cGMP gated channel is composed of homotetramers of the channel protein.

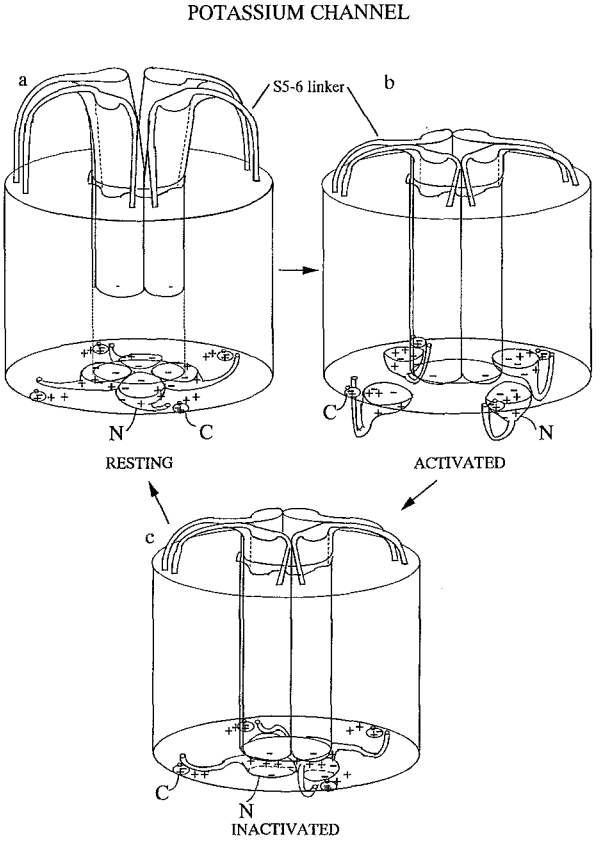

Fig. 12. Schematic illustrations of the potassium channel structure of the resting (*a*), activated (*b*) and inactivated (*c*) states. Potassium channel is composed of homotetramers of the channel protein, and N-tails are connected with each other in the resting state.

18th position, are substituted for the negative ones (Fig. 6*a*). In our model, the negatively charged residues of S4 work to inhibit the gating action of the S5–6 region. cGMP most likely binds to the positively charged residue of the C-tail in cGMP-gated channels (Kaupp et al., 1989). This is quite consistent with the idea of cGMP-gated activation; the cGMP binding induces the conformational change of C-tail, which plugs the center pore in the resting state. Subsequently, the C-tail is strongly attracted by positively charged residues in the N-tail or ones in S2–S3 linkers and S4–S5 linkers (Fig. 11*a, b*). Thus, the cGMP-gated channel is activated (Fig. 11*c*).

Repeat IV of sodium and calcium channels possesses an additional conserved part of S5–6 regions near S6 (Sato & Matsumoto, 1992*b*). This difference may contribute to the functional difference of the sodium and calcium channels and that of cGMP-gated and potassium channels.

S5–6 region of the potassium channel is smaller in its amino acid sequence length than those of other kinds of channels in the same family. Further, it possesses only one or two negatively charged residues in the identical positions where the other channels possess strongly negative charges. Negatively charged residues for ion selective filtering, therefore, might be less in number, and the pore size may be larger than those of Na and Ca channels. Slow inactivation of the potassium channel also can be explained by our octagonal structure model that the channel closes slowly since only the N-terminal region behaves like both III-IV linker and C-terminal region of sodium channel without elastic force (Fig. 12). In the resting state of the potassium channel, the tips of S5–6 regions partially enter into the S2–S4 pore and N-tails are connected with each other to plug the center pore (Fig. 12*a*); Individually localized positioning of positive and negative charges in the N-terminal sequence seems to facilitate the interdomain electric coupling of the residues among N-terminal regions. When the membrane is depolarized, S5–6 regions move toward the cytoplasmic side, and then, N-tails are removed from the cytoplasmic end of the center pore to be anchored to the positively charged residues of S2–3 and S4–5 linkers

(Fig. 12*b*). Another possible site to which the N-tail is anchored is the C-tail. After the activation, local repolarization caused by K current induces the N-tail to the cytoplasmic mouse of the center pore. As a result, N-tails connect with each other to plug the negatively charged S5–6 region as shown in Fig. 12*c*.

In site-directed mutagenesis experiments, the modification of the neutral residue, leucine to valine, in the cytoplasmic side of S4 segment and S4–5 linker all greatly affected both voltage dependency and inactivation of K channel, although the similar modification in the membrane side of S4 did not (McCormack et al., 1991). It suggests the importance of the conformation of the cytoplasmic half of S4 segment and neighbouring S4–5 linker which lies near the cytoplasmic mouth of the center pore in voltage sensing and inactivation. Stocker et al. (1990) reported that the N-terminal difference by alternative splicing of K channel affects not only its inactivation but its sensitivities to 4-amino pyridine, TEA and CTX. These experiments can qualitatively be explained by our octagonal structure model that the electrically repulsive force between N-tail and S5–6 region might influence the conformation of S5–6 region in the activated state and change sensitivity to the toxins.

Quite recently neutralization of the charge of S2 or S3 were revealed to change voltage sensitivity dramatically in the K channel (Planells-Cases et al., 1995). For the mutant potassium channel, where the negative stopping charge of the S2 segment is converted into the positive one, the mutant channel is experimentally found to become sensitive. These findings are quite consistent with our octagonal structure model since this polarity modification to induce the voltage sensitivity change can greatly be effective to the stopping function in the residue of S2. Further, the change of aspartic acid in the 6th position of S3 to other residues most probably makes the channel silent (Planells-Cases et al., 1995). It is in good agreement with our model since the aspartic acid is the key residue in the octagonal structure formation. The *h-erg* K channel, which possesses complete S4 and other transmembrane components S1 through S6 (Warmke & Ganetzky, 1994), was revealed to be an inward rectifier K channel (Trudeau et al., 1995). The number of positive charges in the S4 segment is just the same as that of the *Shaker* K channel in spite of its low voltage sensitivity. In our octagonal structure model, low voltage sensitivity is caused by the lack of negative charge in the S5–6 region and by the existence of negative charge in the 18th position of S4 (Warmke & Ganetzky, 1994). Furthermore, it was found experimentally that deletion of most of the linker between S3 and S4, which seems to inhibit the most outward movement of S4, did not influence the voltage sensitivity significantly (Mathur et al., 1995). These results seem to lend further support to our model that the S4 behaves as the guiding rail rather than as the voltage sensor.

Inward Rectifier Potassium Channel

Recently, molecular cloning of inward rectifier K channels were reported (Kubo et al., 1993*a, b;* Ho et al., 1993). From the amino acid sequence of the inward rectifier K channel gene, they assumed two putative transmembrane segments, M1 and M2 (Ho et al., 1993; Kubo et al., 1993*a*), and one linker which possess homology with S5–6 region (Ho et al., 1993; Kubo et al., 1993*a*). The possibility of MO as a transmembrane segment was also pointed out (Ho et al., 1993). M0 and M2 are shown to have low homology with S4 and S6, respectively (Ho et al., 1993; Kubo et al., 1993*a*). Further, the inward rectifier K channel protein is thought to be composed of an homotetramer and its S5–6 regions to line the center pore (Ho et al., 1993; Kubo et al., 1993*a; see* note added in proof). In the octagonal structure model, these channels are regarded as composing only one octagonal core structure (Fig. 13). M0 and M2 are thought to be located in the corresponding positions of S4 and S2 in the sodium channel, respectively. That is because both M0 and M2 are amphipathic and can face both the center pore and lipid bilayer. M1 is located in the arm of S5–6 region in the membrane side and forms a ball whose inside is hydrophobic (Fig. 13*a, b*). Low-voltage sensitivity may be caused by negative charge in the middle of the rail together with the large gap of positive charges on the rail of M0 in ROMK1, IRK1 and GIRK1, and further by a stopping residue (negatively charged residue) of M2 which lines the inner surface of the center pore in IRK1 and GIRK1, in addition to the only one nomimal negative charge in the S5–6 region (Fig. 13*b*). On depolarization, the channel closes slowly by motion of the M1 region (Fig. 13*d*). The Mg ion, presumably responsible for blocking the inward rectifier K channel, might connect to the C-tail at its strongly negatively charged sites (Fig. 13*c*). The presumed number of transmembrane segments of 8 in functional inward rectifier K channel protein is one of the most affirmative experimental results for the octagonal core structure.

Furthermore, *h-erg* K channel was revealed to be the inward rectifier K channel (Trudeau et al., 1995) in spite of the fact that transmembrane segments S1 through S6 seem normal (Warmke & Ganetzky, 1994). The main difference is on the situation that negative charges lack in the S5–6 regions. It can be easily understood in our octagonal structure model since both types of channels possess the common core structure, thus causing the common mechanisms in voltage sensing.

Relationship of our Model to the Mutation in the Human Sodium Channel Gene

Furthermore, the question raised by Ptáček et al. (1991) as to why substitution of a single residue in the IIS5

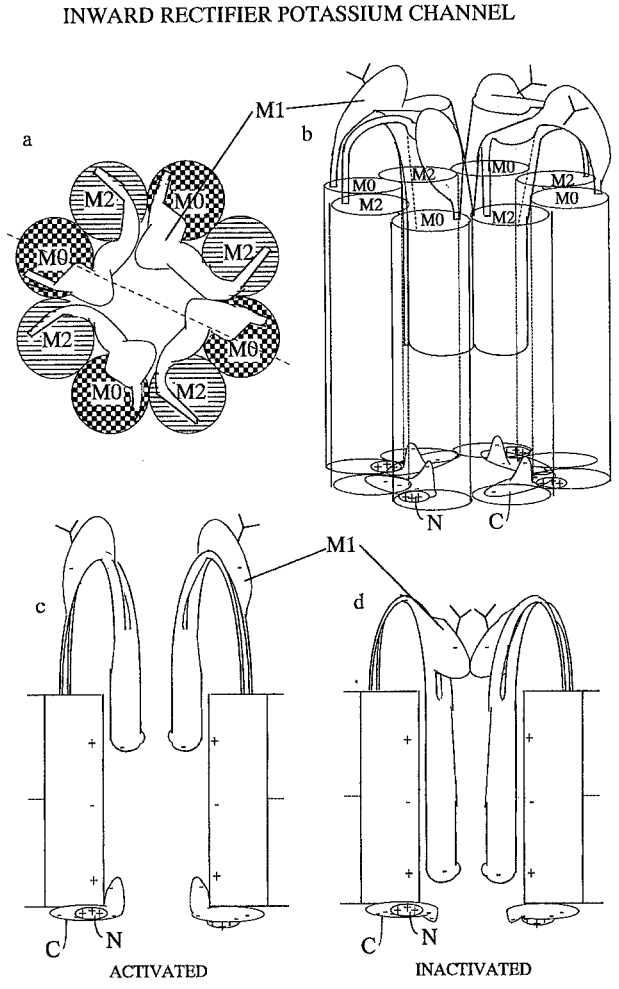

Fig. 13. Schematic illustrations of our proposed tertiary structure model of inward rectifier K channel. Octagonal topology of transmembrane segments M0 and M2 and the S5–6 regions for the homotetramer is shown, as viewed from the extracellular side (*a*) and from the transmembrane side (*b*), respectively. Activated configurations of the S5–6 regions, C- and N-terminals and M1 are also illustrated along dotted line in *a*, where cross sections of the segments M0 (*c*). Resting configuration is also illustrated (*d*). The putative glycosylation site is shown in *b, c, d.*

segment caused hyperkalemic periodic paralysis (HYPP), a disease caused by inactivation deficiency, may be answered by our octagonal configuration model of the sodium channel, where the IIS5 segment is a direct neighbor of the IVS1 segment; that is, in this configuration it may be possible that a single point mutation in the IIS5 segment affects the IVS1 segment, resulting in changes in the elasticity of III–IV linker, which delays the inactivation. HYPP is also reported to affect conductance of the channel (Lehmann-Horn et al., 1991), which might be due to the conformational change of S5–6 region because of the altered interaction between the III–IV linker and the S5–6 region. Paramyotonia congenita (PMC), attributed to the mutation in the III–IV linker (McClatchey et al., 1992), may change the conformation of the III–IV linker directly. The experiments that will determine that exact mechanism are, however, left for the future.

The authors would like to express our cordial acknowledgments to Dr. Hideo Tani (Kowa) and Drs. Masahiko Fujino and Haruo Onda (Takeda Pharmaceutical) for their kind support for us to utilize their experimental facilities for DNA cloning and as well as for their stimulating and helpful discussions. We also thank Drs. Toshio Iijima, Michinori Ichikawa, Kiyonori Hirota, Messrs. Tadashi Kimura and Osamu Shono and all our colleagues (Supermolecular Science Division, Electrotechnical Laboratory) for their kind support to collect and isolate optic lobes from live squid. We greatly thank Professors Takuji Takeuchi (University of Tohoku) and David Landowne (University of Miami) for their illuminating discussions and valuable comments.

Note added in proof: The G-protein-gated atrial K channel I_{KACh} was recently revealed to be heteromultimer (Krapivinsky et al., 1995). The particular sites noted in this model important for ion selectivity and gating conserve their negative and positive charges except for the positive one in the cytoplasmic side of M0.

References

Anderson, P.A.V. 1987. Properties and pharmacology of a TTX-insensitive Na^+ current in neurones of the jellyfish *Cyanea capillata. J. Exp. Biol.* **133:**231–248

Anderson, P.A.V., Holman, M.A., Greenberg, R.M. 1993. Deduced amino acid sequence of a putative sodium channel from the scyphozoan jellyfish *Cyanea capillata. Proc. Natl. Acad. Sci. USA* **90:**7419–7423

Armstrong, C.M., Bezanilla, F. 1974. Charge movement associated with the opening and closing of the activation gates of the Na channels. *J. Gen. Physiol.* **63:**533–552

Armstrong, C.M., Bezanilla, F. 1977. Inactivation of the sodium channel. II. Gating current experiments. *J. Gen. Physiol.* **70:**567–590

Auld, V.J., Goldin, A.L., Krafte, D.S., Catterall, W.A., Lester, H.A., Davidson, N., Dunn, R.J. 1990. A neutral amino acid change in segment IIS4 dramatically alters the gating properties of the voltage-dependent sodium channel. *Proc. Natl. Acad. Sci. USA* **87:**323–327

Baker, P.F., Hodgkin, A.L., Ridgway, E.B. 1971. Depolarization and calcium entry in squid giant axons. *J. Physiol.* **218:**709–755

Bezanilla, F., Armstrong, C.M. 1972. Negative conductance caused by entry of sodium and cesium ions into the potassium channels of squid axons. *J. Gen. Physiol.* **60:**588–608

Bezanilla, F. 1985. Gating of sodium and potassium channels. *J. Membrane Biol.* **88:**97–111

Biel, M., Altenhofen, W., Hullin, R., Ludwig, J., Freichel, M., Flockerzi, V., Dascal, N., Kaupp, U.B., Hofmann, F. 1993. Primary structure and functional expression of a cyclic nucleotide-gated channel from rabbit aorta. *FEBS Lett.* **329:**134–138

Butler, A., Wei, A., Baker, K., Salkoff, L. 1989. A family of putative potassium channel genes in *Drosophila. Science* **243:**943–947

Catterall, W.A., 1979. Binding of scorpion toxin to receptor sites associated with sodium channels in frog muscle. Correlation of voltage-dependent binding with activation. *J. Gen. Physiol.* **74:**375–391

Catterall, W.A., Beneski, D.A. 1981. Biochemical and allosteric properties of neurotoxin receptor site associated with voltage-sensitive

sodium channels, in Nerve membrane. *In:* Biochemistry and function of channel proteins. G. Matsumoto, M. Kotani, editors. pp. 3–11. The University of Tokyo, Tokyo

Catterall, W.A. 1986. Voltage-dependent gating of sodium channels: correlating structure and function. *TINS* **9:**7–10

Chabala, L.D., Urban, B.W., Weiss, L.B., Green, W.N., Andersen, O.S. 1991. Steady-state gating of batrachotoxin-modified sodium channels. Variability and electrolyte-dependent modulation. *J. Gen. Physiol.* **98:**197–224

Chirgwin, J.M., Przybyla, A.E., MacDonald, R.J., Rutter, W.J. 1979. Isolation of biologically active ribonucleic acid from sources enriched in ribonuclease. *Biochemistry* **18:**5294–5299

Conn, E.E., Stump, K.P., Bruening, G., Doi, R.H. 1987. Outlines of biochemistry, Fifth edition. John Wiley & Sons, New York

Dhallan, R.S., Yau, K.-W., Schrader, K.A., Reed, R.R. 1990. Primary structure and functional expression of a cyclic nucleotide-activated channel from olfactory neurons. *Nature* **347:**184–187

Durell, S.R., Guy, H.R. 1992. Atomic scale structure and functional models of voltage-gated potassium channels. *Biophys. J.* **62:**238–250

Frech, G.C., VanDongen, A.M.J., Schuster, G., Brown, A.M., Joho, R.H. 1989. A novel potassium channel with delayed rectifier properties isolated from rat brain by expression cloning. *Nature* **340:**642–645

French, R.J., Wells, J.B. 1977. Sodium ions as blocking agents and charge carriers in the potassium channel of the squid giant axon. *J. Gen. Physiol.* **70:**707–724

Gellens, M.E., George, A.L., Jr., Chen, L., Chahine, M., Horn, R., Barchi, R.L., Kallen, R.G. 1992. Primary structure and functional expression of the human cardiac tetrodotoxin-insensitive voltage-dependent sodium channel. *Proc. Natl. Acad. Sci. USA* **89:**554–558

Guy, H.R., Seetharamulu, P. 1986. Molecular model of the action potential sodium channel. *Proc. Natl. Acad. Sci. USA* **83:**508–512

Heinemann, S.H., Terlau, H., Stühmer, W., Imoto, K., Numa, S. 1992. Calcium channel characteristics conferred on the sodium channel by single mutations. *Nature* **356:**441–443

Hille, B. 1992. Ionic Channels of Excitable Membranes, Second edition. Sinauer, Sunderland, MA

Hironaka, T., Narahashi, T. 1977. Cation permeability ratio of sodium channels in normal and grayanotoxin-treated squid axon membranes. *J. Membrane Biol.* **31:**359–381

Ho, K., Nichols, C.G., Lederer, W.J., Lytton, J., Vassilev, P.M., Kanazirska, M.V., Hebert, S.C. 1993. Cloning and expression of an inwardly rectifying ATP-regulated potassium channel. *Nature* **362:**31–38

Hodgkin, A.L., Huxley, A.F. 1952. A quantitative description of membrane current and its application to conduction and excitation in nerve. *J. Physiol.* **117:**500–544

Hubbard, S.C., Ivatt, R.J. 1981. Synthesis and processing of asparagine-linked oligosaccharides. *Ann. Rev. Biochem.* **50:**555–583

Ichikawa, M., Urayama, M., Matsumoto, G. 1991. Anticalmodulin drugs block the sodium gating current of squid giant axons. *J. Membrane Biol.* **120:**211–222

Ito, H., Morton, T.H., Vodyanoy, V. 1989. Small odorant molecules affect steady state properties of monolayers. *Thin solid Films* **180:**1–13

Jan, L.Y., Jan, Y.N. 1990. A superfamily of ion channels. *Nature* **345:**672

Kaupp, U.B., Niidome, T., Tanabe, T., Terada, S., Bönigk, W., Stühmer, W., Cook, N.J., Kangawa, K., Matsuo, H., Hirose, T., Miyata, T., Numa, S. 1989. Primary structure and functional expression from complementary DNA of the rod photoreceptor cyclic GMP-gated channel. *Nature* **342:**762–766

Kayano, T., Noda, M., Flockerzi, V., Takahashi, H., Numa, S. 1988. Primary structure of rat brain sodium channel III deduced from the cDNA sequence. *FEBS Lett.* **228:**187–194

Keynes, R.D., Greeff, N.G., Forster, I.C., Bekkers, J.M. 1991. The effect of tetrodotoxin on the sodium gating current in the squid giant axon. *Proc. R. Soc. Lond. B* **246:**135–140

Khodorov, B.I. 1978. Chemicals as tools to study nerve fiber sodium channels; effects of batrachotoxin and some anesthetics. *In:* Membrane Transport Processes. D.C. Tosteson, Y.A. Ovchirrikov, R. Latorre. editors. Raven, New York

Kim, M.-S., Morii, T., Sun, L.-X., Imoto, K., Mori, Y. 1993. Structural determinants of ion selectivity in brain calcium channel. *FEBS Lett.* **318:**145–148

Krapivinsky, G., Gordon, E.A., Wickman, K., Velimirović, B., Krapivinsky, L., Clapham, D.E., 1995. The G-protein-gated atrial K^+ channel I_{KACh} is a heteromultimer of two inwardly rectifying K^+ channel proteins. *Nature* **374:**135–141

Kubo, Y., Baldwin, T.J., Jan, Y.N., Jan, L.Y. 1993*a*. Primary structure and functional expression of a mouse inward rectifier potassium channel. *Nature* **362:**127–133

Kubo, Y., Reuveny, E., Slesinger, P.A., Jan, Y.N., Jan, L.Y. 1993*b*. Primary structure and functional expression of a rat G-protein-coupled muscarinic potassium channel. *Nature* **364:**802–806

Kyte, J., Doolittle, R.F. 1982. A simple method for displaying the hydropathic character of a protein. *J. Mol. Biol.* **157:**105–132

Landowne, D. 1993. Measuring nerve excitation with polarized light. *Jap. J. Physiol.* **43:**7–11

Lehmann-Horn, F., Iaizzo, P.A., Hatt, H., Franke, Ch. 1991. Altered gating and conductance of Na^+ channels in hyperkalemic periodic paralysis. *Pfluegers Arch* **418:**297–299

Lewin, B. 1994. The apparatus for nuclear splicing. *In:* Genes V. pp. 911–940. Oxford University, Oxford

Ludwig, J., Margalit, T., Eismann, E., Lancet, D., Kaupp, U.B. 1990. Primary structure of cAMP-gated channel from bovine olfactory epithelium. *FEBS Lett.* **270:**24–29

MacKinnon, R., Yellen, G. 1990. Mutations affecting TEA blockade and ion permeation in voltage-activated K^+ channels. *Science* **250:**276–279

Mathur, R., Zheng, J., Yan, Y., Sigworth, F.J. 1995. Role of the S3–S4 linker in activation of Shaker K^+ channels. *Biophys. J.* **68:**A32

McClatchey, A.I., Van den Bergh, P., Pericak-Vance, M.A., Raskind, W., Verellen, C., Mckenna-Yasek, D., Rao, K., Haines, J.L., Bird, T., Brown, R.H., Jr., Gusella, J.F. 1992. Temperature-sensitive mutations in the III–IV cytoplasmic loop region of the skeletal muscle sodium channel gene in paramyotonia congenita. *Cell* **68:**769–774

McCormack, K., Tanouye, M.A., Iverson, L.E., Lin, J.-W., Ramaswami, M., McCormack, T., Campanelli, J.T., Mathew, M.K., Rudy, B. 1991. A role for hydrophobic residues in the voltage-dependent gating of Shaker K^+ channels. *Proc. Natl. Acad. Sci. USA* **88:**2931–2935

Mikami, A., Imoto, K., Tanabe, T., Niidome, T., Mori, Y., Takeshima, H., Narumiya, S., Numa, S. 1989. Primary structure and functional expression of the cardiac dihydropyridine-sensitive calcium channel. *Nature* **340:**230–233

Miller, I.R. 1993. Mechanism of channel opening and closing: a hypothesis. *Bioelectrochem. Bioenergetics* **31:**323–328

Moorman, J.R., Kirsch, G.E., Brown, A.M., Joho, R.H. 1990. Changes in sodium channel gating produced by point mutations in a cytoplasmic linker. *Science* **250:**688–691

Mori, Y., Friedrich, T., Kim, M.-S., Mikami, A., Nakai, J., Ruth, P., Bosse, E., Hofmann, F., Flockerzi, V., Furuichi, T., Mikoshiba, K., Imoto, K., Tanabe, T., Numa, S. 1991. Primary structure and functional expression from complementary DNA of a brain calcium channel. *Nature* **350:**398–402

Nakayama, H., Hatanaka, Y., Yoshida, E., Oka, K., Takanohashi, M., Amano, Y., Kanaoka, Y. 1992. Photolabeled sites with a tetrodo-

toxin derivative in the domain III and IV of the electroplax sodium channel. *Biochem. Biophys. Res. Comm.* **184:**900–907

Niidome, T., Kim, M.-S., Friedrich, T., Mori, Y. 1992. Molecular cloning and characterization of a novel calcium channel from rabbit brain. *FEBS Lett.* **308:**7–13

Noda, M., Shimizu, S., Tanabe, T., Takai, T., Kayano, T., Ikeda, T., Takahashi H, Nakayama, H., Kanaoka, Y., Minamino, N., Kangawa, K., Matsuo, H., Raftery, M.A., Hirose, T., Inayama, S., Hayashida, H., Miyata, T., Numa, S. 1984. Primary structure of *Electrophorus electricus* sodium channel deduced from cDNA sequence. *Nature* **312:**121–127

Noda, M., Ikeda, T., Kayano, T., Suzuki, H., Takeshima, H., Kurasaki, M., Takahashi, H., Numa, S. 1986. Existence of distinct sodium channel messenger RNAs in rat brain. *Nature* **320:**188–192

Noda, M., Suzuki, H., Numa, S., Stühmer, W. 1989. A single point mutation confers tetrodotoxin and saxitoxin insensitivity on the sodium channel II. *FEBS Lett.* **259:**213–216

Pittler, S.J., Lee, A.K., Altherr, M.R., Howard, T.A., Seldin, M.F., Hurwitz, R.L., Wasmuth, J.J., Baehr, W. 1992. Primary structure and chromosomal localization of human and mouse rod photoreceptor cGMP-gated cation channel. *J. Biol. Chem.* **267:**6257–6262

Planells-Cases, R., Ferrer-Montiel, A.V., Patten, C.D., Montal, M. 1995. The S2 and S3 transmembrane segments are additional components of the voltage sensor in voltage-gated potassium channels. *Biophys. J.* **68:**A34

Ptáček, L.J., George, A.L., Jr., Griggs, R.C., Tawil, R., Kallen, R.G., Barchi, R.L., Robertson, M., Leppert, M.F. 1991. Identification of a mutation in the gene causing hyperkalemic periodic paralysis. *Cell* **67:**1021–1027

Pusch, M., Noda, M., Stühmer, W., Numa, S., Conti, F. 1991. Single point mutations of the sodium channel drastically reduce the pore permeability without preventing its gating. *Eur. Biophys. J.* **20:**127–133

Rogart, R.B., Cribbs, L.L., Muglia, L.K., Kephart, D.D., Kaiser, M.W. 1989. Molecular cloning of a putative tetrodotoxin-resistant rat heart Na^+ channel isoform. *Proc. Natl. Acad. Sci. USA* **86:**8170–8174

Rosenthal, J.J.C., Gilly, W.F. 1993. Amino acid sequence of a putative sodium channel expressed in the giant axon of the squid *Loligo opalescens. Proc. Natl. Acad. Sci USA* **90:**10026–10030

Saiki, R.K., Scharf, S., Faloona, F., Mullis, K.B., Horn, G.T., Erlich, H.A., Arnheim, N. 1985. Enzymatic amplification of β-globin genomic sequences and restriction site analysis for diagnosis of sickle cell anemia. *Science* **230:**1350–1354

Saiki, R.K., Gelfand, D.H., Stoffel, S., Scharf, S.J., Higuchi, R., Horn, G.T., Mullis, K.B., Erlich, H.A. 1988. Primer-directed enzymatic amplification of DNA with a thermostable DNA polymerase. *Science* **239:**487–491

Salkoff, L., Butler, A., Wei, A., Scavarda, N., Giffen, K., Ifune, C., Goodman, R., Mandel, G. 1987. Genomic organization and deduced amino acid sequence of a putative sodium channel gene in *Drosophila. Science* **237:**744–749

Satin, J., Kyle, J.W., Chen, M., Bell, P., Cribbs, L.L., Fozzard, H.A., Rogart, R.B. 1992. A mutant of TTX-resistant cardiac sodium channels with TTX-sensitive properties. *Science* **256:**1202–1205

Sato, C., Matsumoto, G. 1992*a*. Primary structure of squid sodium channel deduced from the complementary DNA sequence. *Biochem. Biophys. Res. Comm.* **186:**61–68

Sato, C., Matsumoto, G. 1992*b*. Proposed tertiary structure of the sodium channel. *Biochem. Biophys. Res. Comm.* **186:**1158–1167

Sato, C., Hirota, K., Matsumoto, G. 1995. Neuronal specificity of subtype SQSC1 of squid putative sodium channel. *Biochem. Biophys. Res. Comm.* **206:**807–813

Stocker, M., Stühmer, W., Wittka, R., Wang, X., Müller, R., Ferrus, A., Pongs, O. 1990. Alternative *Shaker* transcripts express either rapidly inactivating or noninactivating K^+ channels. *Proc. Natl. Acad. Sci. USA* **87:**8903–8907

Stühmer, W., Conti, F., Suzuki, H., Wang, X., Noda, M., Yahagi, N., Kubo, H., Numa, S. 1989. Structural parts involved in activation and inactivation of the sodium channel. *Nature* **339:**597–603

Tanabe, T., Takeshima, H., Mikami, A., Flockerzi, V., Takahashi, H., Kangawa, K., Kojima, M., Matsuo, H., Hirose, T., Numa, S. 1987. Primary structure of the receptor for calcium channel blockers from skeletal muscle. *Nature* **328:**313–318

Tang, S., Mikala, G., Bahinski, A., Yatani, A., Varadi, G., Schwartz, A. 1993. Molecular localization of ion selectivity sites within the pore of a human L-type cardiac calcium channel. *J. Biol. Chem.* **268:**13026–13029

Tejedor, F.J., Catterall, W.A. 1988. Site of covalent attachment of α-scorpion toxin derivatives in domain I of the sodium channel α subunit. *Proc. Natl. Acad. Sci USA* **85:**8742–8746

Tempel, B.L., Papazian, D.M., Schwarz, T.L., Jan, Y.N., Jan, L.Y. 1987. Sequence of a probable potassium channel component encoded at *Shaker* Locus of *Drosophila. Science* **237:**770–775

Tempel, B.L., Jan, Y.N., Jan, L.Y. 1988. Cloning of a probable potassium channel gene from mouse brain. *Nature* **332:**837–839

Terlau, H., Heinemann, S.H., Stühmer, W., Pusch, M., Conti, F., Imoto, K., Numa, S. 1991. Mapping the site of block by tetrodotoxin and saxitoxin of sodium channel II. *FEBS Lett.* **293:**93–96

Thomsen, W.J., Catterall, W.A. 1989. Localization of the receptor site for α-scorpion toxins by antibody mapping: Implications for sodium channel topology. *Proc. Natl. Acad. Sci. USA* **86:**10161–10165

Triglia, T., Peterson, M.G., Kemp, D.J. 1988. A procedure for in vitro amplification of DNA segments that lie outside the boundaries of known sequences. *Nucleic Acids Res.* **16:**8186

Trimmer, J.S., Cooperman, S.S., Tomiko, S.A., Zhou, J., Crean, S.M., Boyle, M.B., Kallen, R.G., Sheng, Z., Barchi, R.L., Sigworth, F.J., Goodman, R.H., Agnew, W.S., Mandel, G. 1989. Primary structure and functional expression of a mammalian skeletal muscle sodium channel. *Neuron* **3:**33–49

Trimmer, J.S., Agnew, W.S. 1989. Molecular diversity of voltage-sensitive Na channels. *Annu. Rev. Physiol.* **51:**401–418

Trudeau, M.C., Warmke, J.W., Ganetzky, B., Robertson, G.A. 1995. H-erg, a member of the eag family of K^+ channels, encodes an inward rectifier. *Biophys. J.* **68:**A32

Tsuji, K., Kawanishi, T., Handa, S., Kamano, H., Iwasa, J., Seyama, I. 1991. Effect of structural modification of several groups on the D-ring of grayanotoxin on its depolarization potency in squid giant axon. *J. Pharmacol. Exp. Ther.* **257:**788–794

Tsukita, S., Tsukita, S., Kobayashi, T., Matsumoto, G. 1986. Subaxolemmal cytoskeleton in squid giant axon. II. Morphological identification of microtubule-and microfilament-associated domains of axolemma. *J. Cell Biol.* **102:**1710–1725

Vale, R.D., Schnapp, B.J., Reese, T.S., Sheetz, M.P. 1985. Movement of organelles along filaments dissociated from the axoplasm of the squid giant axon. *Cell* **40:**449–454

Vassilev, P.M., Scheuer, T., Catterall, W.A. 1988. Identification of an intracellular peptide segment involved in sodium channel inactivation. *Science* **241:**1658–1661

Warmke, J.W., Ganetzky, B. 1994. A family of potassium channel genes related to eag in *Drosophila* and mammals. *Proc. Natl. Acad. Sci. USA.* **91:**3438–3442

Waugh, R.E., Hochmuth, R.M. 1987. Mechanical equilibrium of thick, hollow, liquid membrane cylinders. *Biophys. J.* **52:**391–400

Waugh, R.E., Song, J., Svetina, S., Žekš, B. 1992. Local and nonlocal

curvature elasticity in bilayer membranes by tether formation from lecithin vesicles. *Biophys. J.* **61:**974–982

Wei, A., Covarrubias, M., Butler, A., Baker, K., Pak, M., Salkoff, L. 1990. K^+ current diversity is produced by an extended gene family conserved in *Drosophila* and mouse. *Science* **248:**599–603

West, J.W., Numann, R., Murphy, B.J., Scheuer, T., Catterall, W.A. 1991. A phosphorylation site in the Na^+ channel required for modulation by protein kinase C. *Science* **254:**866–868

West, J.W., Patton, D.E., Scheuer, T., Wang, Y., Goldin, A.L., Catterall, W.A. 1992. A cluster of hydrophobic amino acid residues required for fast Na^+-channel inactivation. *Proc. Natl. Acad. Sci. USA.* **89:**10910–10914

Yellen, G., Jurman, M.E., Abramson, T., MacKinnon, R. 1991. Mutations affecting internal TEA blockade identify the probable pore-forming region of a K^+ channel. *Science* **251:**939–942

Yokoyama, S., Imoto, K., Kawamura, T., Higashida, H., Iwabe, N., Miyata, T., Numa, S. 1989. Potassium channels from NG108–15 neuroblastoma-glioma hybrid cells. Primary structure and functional expression from cDNAs. *FEBS Lett.* **259:**37–42